

# A framework for model-assisted $T \times E \times M$ exploration in maize

Jennifer Hsiao<sup>1</sup>, Soo-Hyung Kim<sup>3</sup>, Dennis J. Timlin<sup>4</sup>, Nathaniel D. Mueller<sup>5</sup>, and Abigail L.S. Swann<sup>1,2</sup>

<sup>1</sup>University of Washington, Department of Biology, Seattle, WA, United States

<sup>2</sup>University of Washington, Department of Biology, Department of Atmospheric Sciences, Seattle, WA, United States

<sup>3</sup>University of Washington, School of Environmental and Forest Sciences, Seattle, WA, United States

<sup>4</sup>USDA-ARS Adaptive Cropping Systems Laboratory, Beltsville, MD, United States

<sup>5</sup>Colorado State University, Department of Ecosystem Science and Sustainability and Department of Soil and Crop Sciences, Fort Collins, CO, United States

June 9, 2022

## Abstract

Breeding for new crop characteristics and adjusting management practices are critical avenues to mitigate yield loss and maintain yield stability under a changing climate. However, identifying high-performing plant traits and management options for different growing regions through traditional breeding practices and agronomic field trials is often time and resource-intensive. Mechanistic crop simulation models can serve as powerful tools to help synthesize cropping information, set breeding targets, and develop adaptation strategies to sustain food production. In this study, we develop a modeling framework for a mechanistic crop model (MAIZSIM) to run many simulations within a trait  $\times$  environment  $\times$  management landscape and demonstrate how such a modeling framework could be used to identify ideal trait-management combinations that maximize yield and yield stability for different agro-climate regions in the US.

## 1 Introduction

Food demand is increasing but our ability to sustain crop productivity will be impacted by a warming climate. Breeding has consistently played a critical role

in the progress of continuous yield gain and was estimated to account for up to 50-60% of the total on-farm yield gain in the past several decades (Duvick, 2005). These gains through genetic improvements are complemented by changes in management practices, such as an increase in fertilizer use, chemical weed control, higher planting densities, and earlier planting dates (Cardwell, 1982; Kucharik, 2008). Recently, however, practices such as nitrogen application and weed control are nearly fully exploited in the US corn belt; simple adjustments in management strategies alone are likely insufficient to sustain an increasing yield trend. Additional yield gains would need to rely further on genetic improvements in new cultivars, as well as management changes that accompany climate-resilient characteristics to fully leverage the interactions among genetics, environment, and management (the  $G \times E \times M$  paradigm, Hatfield and Walthall, 2015).

Continued development of new cultivars better-suited for future climate is critical for sustaining current yield trends or to prevent yield loss (Burke et al., 2009; Challinor et al., 2017). Progress in breeding for climate adaptation has been demonstrated in several areas, including changes in morphological traits (e.g. improved root system architecture that improves soil water access; G. L. Hammer et al., 2009), increases in drought and salinity tolerance (Fita et al., 2015; Messina, Cooper, Hammer, et al., 2020), improvements in physiological traits (e.g. greater nitrogen use efficiency; Fischer and Edmeades, 2010), and shifts in cropping duration (Zhu et al., 2018), to name a few. Our ability to utilize the genetic diversity preserved in wild relatives, landrace species, and undomesticated wild species to develop new climate-ready cultivars is increasingly important to achieve sustainable and intensified food production (Godfray et al., 2010; McCouch et al., 2013).

Maize trait changes in the past few decades have also been accompanied by shifts in crop management practices, such as more erect plant forms that facilitated notable increases in planting densities (Duvick, 2005), shifts towards earlier planting dates by about 3 days per decade (Butler et al., 2018; Zhu et al., 2018), increases in nutrient supply (Duvick, 2005), and increases in area irrigated (Mueller et al., 2016). In addition, the suitability of a cultivar often varies considerably across environmental gradients (e.g. Messina et al., 2015), thus optimal plant traits and management options are usually identified within defined target environments (Cooper et al., 2016). This breeding strategy allows for designing different cultivars to perform favorably and withstand stresses in their target environments, and what is considered “ideal” may differ between locations and climate. We expect optimal management to shift under future climate conditions and in combination with different phenotypic traits, providing important means of adaptation in many systems (Deryng et al., 2011).

Mechanistic modeling tools that integrate physiological, morphological, and phenological properties of a crop ( $G$ ), their performance under different management options ( $M$ ), and their interactions with the surrounding environment ( $E$ ) on a whole-plant level can serve as useful tools for breeding practices through the quantification of a yield-trait-performance landscape (Messina et al., 2011). The structure of such models allow for testing effects of traits (e.g. leaf elongation rate, total leaf number) on integrated outcomes such as yield. While mechanistic crop

models may not specifically describe genetic-level properties, higher-level traits are often used as proxies to describe the underlying genotype. This makes models ideal tools to test and screen for potentially promising traits and management ( $T \times M$ ) combinations under different climate and environmental conditions ( $E$ ) as a first step before carrying out actual breeding practices (Andrison et al., 2012; Messina et al., 2011), and on large scales that are often not feasible under actual experimental settings (Cooper et al., 2020; G. Hammer et al., 2020; B. Peng et al., 2020). Such information can further be used to synthesize cropping knowledge, set breeding targets, and develop climate-targeted adaptation strategies to sustain food production.

Despite broad recognition that mechanistic, process-based crop simulation models can be a powerful tool to synthesize cropping information, set breeding targets for developing climate-ready crops, and develop adaptation strategies for sustaining food production (Messina, Cooper, Hammer, et al., 2020; Muller & Martre, 2019), few comprehensive studies have been performed to produce climate-specific trait and management combinations for staple crops including maize in the US, a necessity given rapidly changing environmental conditions facing the US cropping systems. In this study, we construct a modeling framework to identify targeted plant traits and effective crop management to achieve maximum crop performance in both the current and future climates. Specifically, we addressed how an ensemble of plant traits (i.e. physiology, morphology, phenology) combined with realistic adjustments to management choices (i.e. shifting planting dates, planting density, and row spacing) can be used to build resilience and improve productivity under the stresses induced from a changing climate.

## 2 Material and methods

We set up a data-model framework to quantitatively identify high performing regions within a  $T \times E \times M$  landscape. The framework consists of three main components (Fig. 1): 1) a process-based crop simulation model (section 2.1), 2) model inputs to drive the model, including present-day climate information (section 2.2), idealized future climate information (section 2.3), simulation site soil information (section 2.4), and sampled trait and management options (section 2.5), and 3) processed model outputs that identify performance within the  $T \times E \times M$  landscape (section 2.6 - 2.7), and summarized in-season growth outputs (section 2.8).

### 2.1 Process-based crop simulation model - MAZSIM

MAZSIM is a deterministic and dynamic model developed and calibrated for maize plants to represent key physiological and physical processes such as gas exchange, canopy radiative transfer, carbon partitioning, water relations, nitrogen dynamics and phenology (Kim et al., 2012). MAZSIM interfaces with a 2-dimensional finite element model (2DSOIL) that simulates a dynamic soil

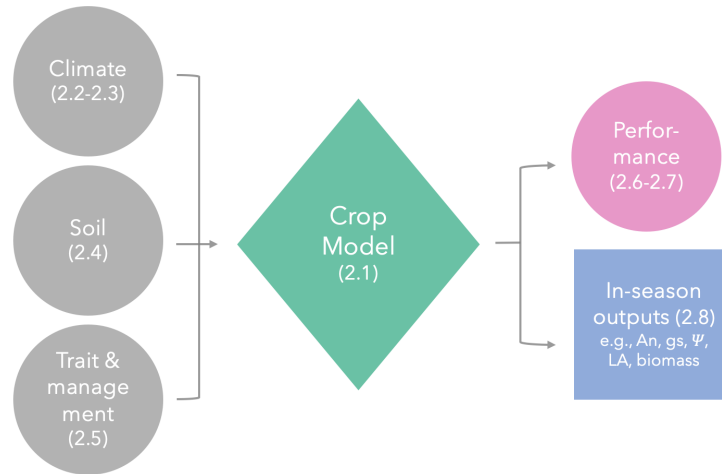


Figure 1: Diagram of the data-model framework.

water and nutrient vertical 2D profile (Timlin et al., 1996). The coupled model responds to daily or hourly meteorological information throughout the growing season that includes temperature, relative humidity, solar radiation, and CO<sub>2</sub> concentrations.

At the leaf-level, MAZSIM captures gas exchange processes through a C4 photosynthesis model (von Caemmerer, 2000) coupled with a stomatal conductance model (Ball et al., 1987) and an energy balance equation (Collatz et al., 1992); leaf-level gas exchange processes are scaled to canopy-levels using a sunlit/shaded leaf framework (de Pury & Farquhar, 1997). The model simulates crop development throughout the growing season following a nonlinear temperature response (Yin et al., 1995), and adopts a leaf area model developed by Lizaso et al., 2003 to describe the expansion and senescence of individual leaves. MAZSIM dynamically simulates leaf water potential and uses it to trigger water stress responses such as reduced growth rate and hastened senescence when values drop below designated thresholds (Yang, Timlin, et al., 2009).

The model has been validated at different scales – including physiological aspects such as gas exchange (Yang, Kim, et al., 2009), leaf development and biomass gain (Kim et al., 2012), leaf growth water stress responses (Yang, Timlin, et al., 2009), as well as field-level validations in AgMIP projects (Bassu et al., 2014; Kimball et al., 2019) and FACE site studies (Durand et al., 2018) that tested for yield responses to different temperature and CO<sub>2</sub> conditions. The model has also recently been used to test the independent impacts of temperature versus VPD on growth and yield in maize growing regions in the US (Hsiao et al., 2019).

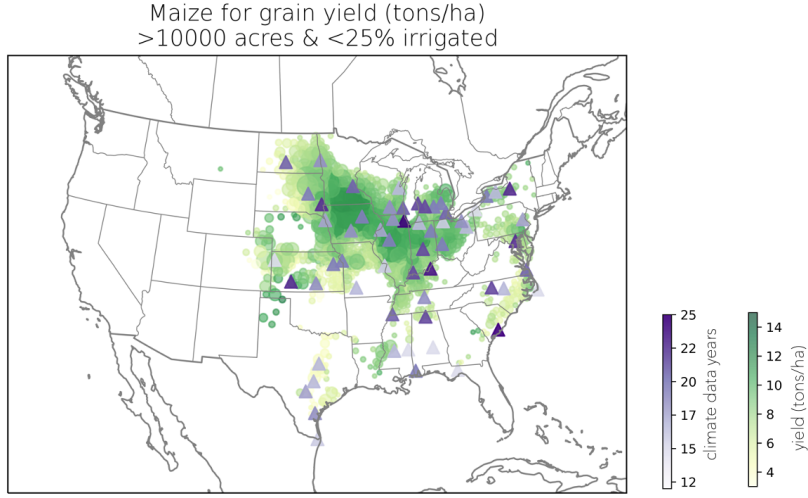


Figure 2: Simulation sites and number of years simulated (purple triangles), along with historic maize yield and planting area data (green circles). Colors indicate yield and circle size indicate planting area.

## 2.2 Present-day climate data

We assembled hourly data of temperature, relative humidity, precipitation, and solar radiation over years 1961-2005 for our simulation sites as weather data input for our model simulations. Specifically, we accessed hourly air temperature ( $T_{air}$ ), dew point temperature ( $T_{dew}$ ), and precipitation data from the NOAA National Center for Environmental Information Integrated Surface Hourly database (<https://www.ncdc.noaa.gov/isd>), and hourly solar radiation data from the National Solar Radiation Data Base (<https://nsrdb.nrel.gov/data-sets/archives.html>).

We followed the Clausius-Clapeyron equation (Eqn. 1-2) to back out atmospheric humidity information in the form of relative humidity (RH) from  $T_{air}$  and  $T_{dew}$ :

$$E_s = E_{sref} \cdot e^{\frac{L_v}{R_v} \cdot (\frac{1}{T_{ref}} - \frac{1}{T_{air}})} \quad (1)$$

$$E = E_{sref} \cdot e^{\frac{L_v}{R_v} \cdot (\frac{1}{T_{ref}} - \frac{1}{T_{dew}})} \quad (2)$$

The equation uses the saturation vapor pressure ( $E_{sref}$ , 6.11 mb) at a reference temperature ( $T_{ref}$ , 273.15 K), the vaporization latent heat ( $L_v$ ,  $2.5 \cdot 10^6$  J kg<sup>-1</sup>), and the gas constant ( $R_v$ , 461 J K<sup>-1</sup>kg<sup>-1</sup>) to calculate the saturated water vapor pressure ( $E_s$ , mb) and the actual water vapor pressure ( $E$ , mb) at air temperature ( $T_{air}$ , K). We then use  $E$  and  $E_s$  to calculate  $RH$  (%) (Eqn. 3):

$$RH = \frac{E}{E_s} \quad (3)$$

We selected overlapping sites and years that had data available from both the Integrated Surface Hourly Data Base and the National Solar Radiation Data Base over years 1961-2005 and filtered for site-years that had less than two consecutive hours of missing data throughout the growing season (broadly defined to be between February 1<sup>st</sup> – November 30<sup>th</sup>) and retained at least two-thirds of the weather data (Fig. S1). We then gap-filled any missing data by linearly interpolating the missing information with weather data of the hours prior and post the missing data point. Next, we linked valid weather stations with maize planting area and irrigation level data accessed through the United States Department of Agriculture – National Agriculture Statistics Service (USDA-NASS, [https://www.nass.usda.gov/Data\\_and\\_Statistics/index.php](https://www.nass.usda.gov/Data_and_Statistics/index.php)). Specifically, we calculated the average maize planting area across our simulation period (1961-2005) in the continental US and accessed average irrigation level (%) for the same sites through four available census years (1997, 2002, 2007, 2012) (Fig. S2). We used the planting area and irrigation level averaged across five USDA-NASS sites closest to each weather station (via Euclidean distance) to represent their cropping information, and to exclude sites that either had less than 10,000 acres of corn planted or had greater than 25 % of crop land irrigated. We excluded sites with less than 15 years of data to insure sufficient sampling to assess inter-annual climate variability (Soltani & Hoogenboom, 2003; Van Wart et al., 2013). Following this method, we were able to compile 1160 site-years of meteorology data for our simulations, which included a total of 60 sites, each site with available weather data ranging from 15-27 years (Fig. 2).

### 2.3 Idealized projected climate

We assembled idealized projected climate information at two future time points, 2050 and 2100, to analyze crop performance shifts under future climate (Table 1). Specifically, we created monthly temperature and relative humidity anomaly maps under a substantial but not extreme greenhouse gas emissions scenario (SSP3-7.0, Riahi et al., 2017) from the latest Coupled Model Intercomparison Project version 6 (CMIP6) outputs; we used these anomaly maps to calculate location-specific warming and associated changes in relative humidity levels throughout the growing season for each simulation site (Fig. 3). This method preserves correlations between climate variables (i.e., between temperature, relative humidity, and solar radiation) on short timescales and limits known biases in modeled variability (Donat et al., 2017; Vargas Zeppetello et al., 2019). Since both magnitude and pattern of future precipitation projections are highly uncertain, we applied a general trend of precipitation reduction in accordance to the SSP3-7.0 scenario, and increased atmospheric concentrations of CO<sub>2</sub> to 550 ppm and 850 ppm for years 2050 and 2100, respectively (O’Neill et al., 2016).

### 2.4 Soil data

We used soil information from USDA-NASS locations nearby our simulation sites to curate site-specific soil files for each location. Soil properties are highly

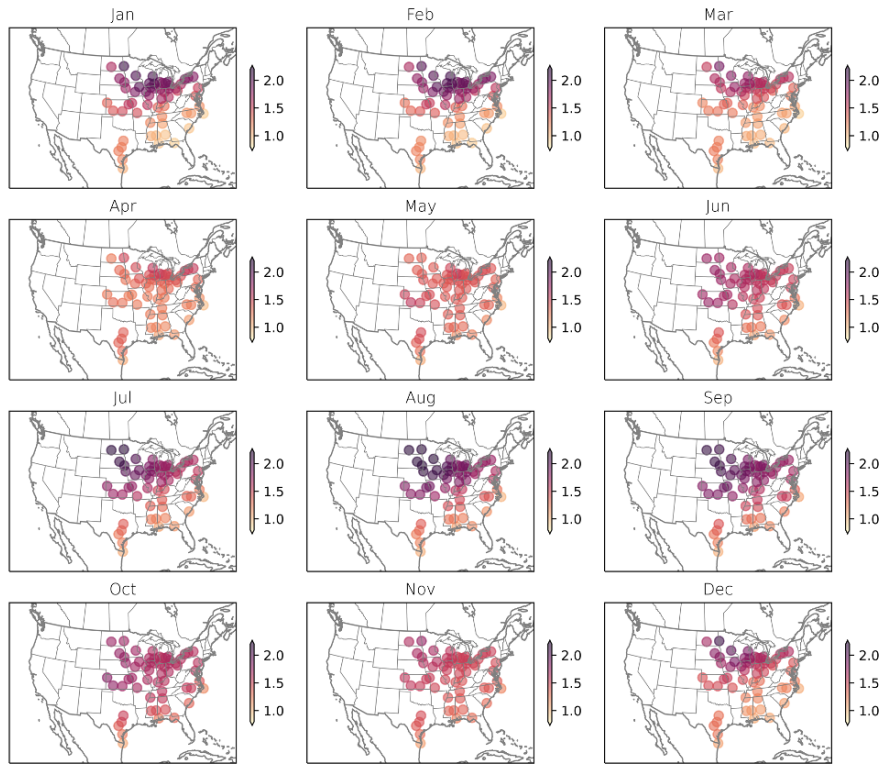


Figure 3: Monthly pattern of warming derived from CMIP6 multimodel means for our simulation sites. Numbers in color bar indicate temperature scaling values to multiply with global average climate sensitivity to calculate projected warming for each simulation site. For example, under our assumption of  $3.1^{\circ}\text{C}$  global average warming by 2100, a scaling value of 2 for a specific simulation site will equal a total warming of  $6.2^{\circ}\text{C}$  for that location.

Table 1: Description of idealized climate treatments with projected changes in temperature (T), relative humidity (RH), precipitation (precip.), and projected CO<sub>2</sub> concentrations by years 2050 and 2100 under the SSP3-7.0 emission scenario.

Year	Climate Scenario
2050	+ 1.4 °C mean T, -RH, -15% precip, 550 ppm
2100	+ 3.1 °C mean T, -RH, -30% precip, 850 ppm

heterogeneous, and since our simulation sites are based on weather station locations that do not directly come from agricultural land, we use this method to broadly represent soil makeup of agricultural sites within the region without skewing towards any particular site. We queried soil information from the National Resources of Conservation Services (NRCS) SSURGO soil database (Soil Survey Staff, n.d.) to identify soil properties for each NASS location with maize planting area greater than 10000 acres and irrigation levels less than 25%. For each site, we accessed soil information at five depth categories (surface, 50, 100, 150, and 200 cm), which included sand–silt–clay–organic matter composition, soil bulk density (the oven dry weight of less than 2 mm soil material per unit volume of soil at a water tension of 1/3 bar), and the volumetric content of soil water retained at a tension of 1/3 bar (33 kPa, field capacity) and 15 bar (1500 kPa, wilting point) expressed as a percentage of the whole soil. With the sand–silt–clay composition, we categorized the queried soil data into 12 texture groups following the USDA Textural Soil Classification (Staff, 1999) and excluded sites classified as Sandy or Clay due to their lack of representation in agricultural fields. Next, we determined the soil class within each depth category for all our simulation sites by assigning it the most prevalent soil class from its 11 nearest NASS sites calculated through Euclidean distance, and assigned it the mean soil conditions of that texture–depth class averaged across all NASS sites within that category. Finally, we estimated soil hydraulic properties of each soil type through a water release curve predicted by the van Genuchten equation (van Genuchten, 1980).

## 2.5 Sampling within the trait and management space

We selected several key model parameters that represent a range of maize traits and management options to investigate combinations that lead to high performance under present and future climate conditions. Since we do not have robust observation-based data on the natural distribution and boundaries of most parameters, we assumed a uniform distribution and set biologically reasonable boundaries around literature-based default values (Table 2). We assumed all parameters to be non-correlated and used a Latin hypercube sampling method (McKay et al., 1979) to create 100 different trait–management ( $T \times M$ ) combinations within the parameter space.



Table 2: MAZSIM parameters tested for yield optimization

Processes	Params	Description	Default (Range)	Citation
Physiology	g1	Ball-Berry $g_s$ model slope	4 (2~6)	Miner et al., 2017; Shekoofa et al., 2016
	$V_{cmax}$	Max RUBISCO capacity	65 (65~80)	Kim et al., 2006; Wu et al., 2019
	$J_{max}$ phyf	Max electron transport rate Reference leaf water potential (MPa) used to describe stomata sensitivity to leaf water potential	350 (350~420) -1.9 (-3~-1)	Kim et al., 2006; Wu et al., 2019 Shekoofa et al., 2016; Tuzet et al., 2003; Yang, Kim, et al., 2009
Phenology	SG	Duration that leaves maintain ac- tive function (stay-green) after reaching maturity	3 (2~6)	Gregersen et al., 2013; Timlin et al., 2019; Zhang et al., 2019
	gleaf	Total leaf number	19 (11~25)	Padilla and Otegui, 2005; Parent et al., 2018
Morphology	LTAR	Max leaf tip appearance rate (leaves/day)	0.5 (0.4~0.8)	Kim et al., 2012; Padilla and Otegui, 2005
	LM	Leaf length of the longest leaf (cm)	115 (80~120)	
	LAF	Leaf angle factor	1.37 (0.9~1.4)	Campbell, 1986; Dzievit et al., 2019
Management	gdd	Growing degree days accumu- lated by sowing	100 (80~160)	Sacks and Kucharik, 2011; Timlin et al., 2019
	pop	Density (plants/m <sup>2</sup> )	8 (6~10)	Stone et al., 2000; Timlin et al., 2019

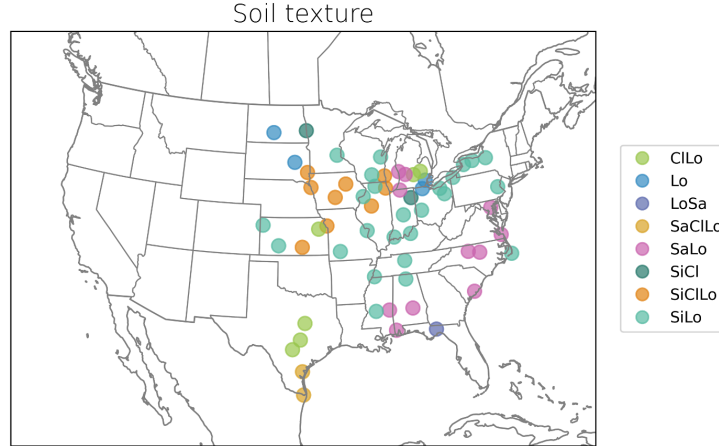


Figure 4: Soil texture across simulation sites. Soil texture categories include clay loam (CILo), loam (Lo), loamy sand (LoSa), sandy clay loam (SaLoLo), sandy loam (SaLo), silty clay (SiCl), silty clay loam (SiCLo), and silty loam (SiLo).

## 2.6 Performance within the $T \times E \times M$ landscape

We defined high crop performance as crops that achieve high yield (i.e. yield mean across years) and high yield stability (i.e. yield dispersion across years). We developed a cost function (Eqn. 4) to quantify the performance of any  $T \times M$  combination by calculating its distance to a theoretical best-performing combination within the yield and yield stability space (Eqn. 4):

$$D_{score} = \sqrt{w_{yield} * (y_{mean} - y_{max})^2 + w_{disp} * (y_{disp} - d_{min})^2} \quad (4)$$

$y_{mean}$  and  $y_{disp}$  represent mean yield and yield dispersion (variance/mean) across years for the target  $T \times M$  combination at a specific simulation site, respectively. We standardized yield and dispersion to values between 0 and 1 to avoid skewed contribution due to difference in scale.  $y_{max}$  and  $d_{min}$  denote the standardized maximum mean yield (1) and minimum yield dispersion (i.e., maximum yield stability, 0) achieved within all  $T \times M$  combinations at a specific simulation site.  $w_{yield}$  and  $w_{disp}$  are empirical coefficients between 0 and 1 that assign weighted importance to yield mean and yield dispersion, respectively.

We used the calculated  $D_{score}$  to rank the top 20 performing  $T \times M$  combinations for each simulation site. We determined an overall ranking for each  $T \times M$  combination based on their rankings across all simulation sites (Fig. 5a). With this method,  $T \times M$  combinations with high rankings across a few sites versus combinations with medium ranking across several sites can all result in overall high performance.  $T \times M$  combinations that do not rank within the top 20 performers at any site will not receive a ranking.

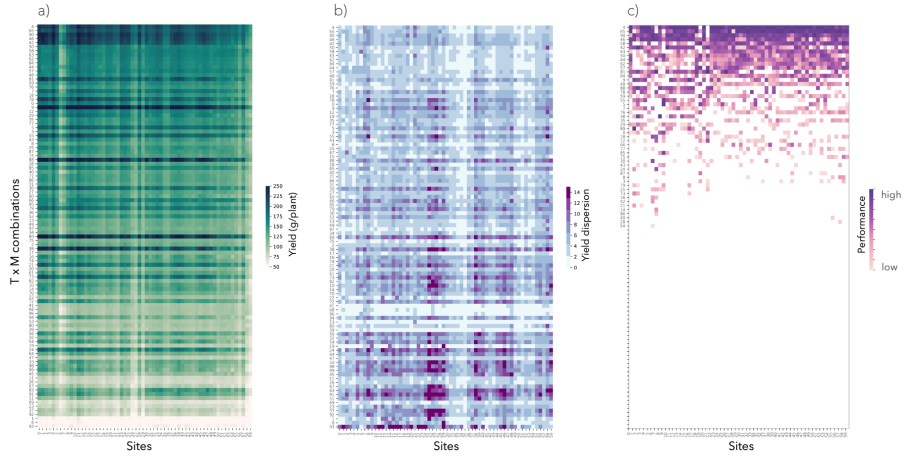


Figure 5: Simulated a) yield, b) yield dispersion, and c) performance ranking of across  $T \times M$  combinations and locations.  $T \times M$  combinations are ordered from top to bottom starting from the highest performance ranking. Sites are order from left to right from sites located in the south to the north.

## 2.7 Regional difference in performance

We used a climate space approach to identify how the performance of  $T \times M$  combinations differed with baseline climate conditions. We used a k-means clustering algorithm to cluster our sites based on mean growing season temperature and VPD, and total growing season precipitation, roughly dividing our simulation sites into four groups of climate spaces - cool and medium precip, mild, warm and wet, and warm and mild to dry (Fig. 6). We analyzed the performance of  $T \times M$  combinations within each cluster of sites by calculating a standardized performance score (Eqn. 5):

$$P_{score} = \frac{\sum_{i=1}^n R_i}{R_{max} * n} \quad (5)$$

$R_i$  denotes the performance ranking of a  $T \times M$  combination at site  $i$  among a total of  $n$  sites within each climate space, and  $R_{max}$  indicates the maximum performance ranking a  $T \times M$  combination can achieve at a single site. In our workflow, we only considered the top 20 performing  $T \times M$  combinations when ranking high performing combinations (see section 2.6), so  $R_{max}$  equals 20. The resulting standardized performance score ranges between 0 and 1, in which a  $T \times M$  combination that ranks with highest in performance across all locations within the climate space would receive a  $P_{score}$  of 1.

## 2.8 In-season model outputs

MAIZSIM generates outputs of a number of plant growth outputs throughout the growing season on an hourly time step. We describe in Table 3 a select

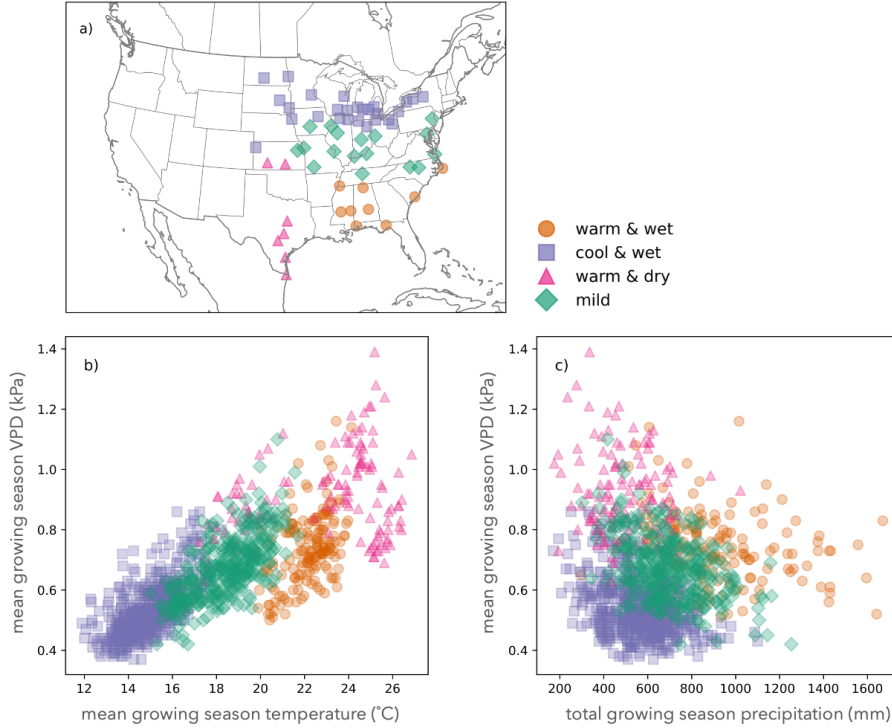


Figure 6: a) Map of simulation sites clustered based on mean growing season temperature ( $^{\circ}\text{C}$ ), mean growing season VPD (kPa), and total growing season precipitation (mm). Mean growing season temperature ( $^{\circ}\text{C}$ ), mean growing season VPD (kPa), and total growing season precipitation (mm) levels for all simulated site-years (b, c).

few outputs in more detail. We summarized these high time frequency outputs across four phenological stages (emerged, tassel initiation, tasseled and silked, and grain-filling) to facilitate analysis and interpretation. Specifically, we queried net photosynthetic rate ( $A_n$ ), net carbon gain ( $P_n$ ), and stomatal conductance ( $g_s$ ) values from daylight hours, and averaged them within the designated phenological stages. We represented ear biomass, total biomass, and total leaf area ( $ear\_biomass$ ,  $total\_biomass$ ,  $LA$ ) within each developmental stage with maximum values within each stage. Finally, we queried water supply, demand, and deficit ( $ET\_supply$ ,  $ET\_demand$ ,  $water\_deficit$ ) values at noon and averaged all values within each phenological stage, and represented predawn leaf water potential ( $\Psi$ ) with values queried at 5 am, and averaged the all values within each phenological stage.

Table 3: Key model outputs

Output	Description	Unit
$A_n$	Net photosynthetic rate	$\mu\text{mol CO}_2 \text{ m}^{-2} \text{ sec}^{-1}$
$P_n$	Net carbon gain	g /plant hour
$g_s$	Stomatal conductance	$\text{g H}_2\text{O m}^{-2} \text{ sec}^{-1}$
<i>ear_biomass</i>	Total ear biomass	g/plant
<i>total_biomass</i>	Total plant biomass	g/plant
<i>LA</i>	Total leaf area	$\text{cm}^2$
<i>phenostage</i>	Phenological stage	-
<i>ET_supply</i>	Evapotranspiration (ET) supply	g H <sub>2</sub> O
<i>ET_demand</i>	Evapotranspiration demand	g H <sub>2</sub> O
<i>water_deficit</i>	ET demand - ET supply	g H <sub>2</sub> O
$\Psi$	Leaf water potential	MPa

## 2.9 Experiment setup and model simulation

We prescribed the sampled planting density (Table 2, *pop*) for each ensemble member and adjusted the planting date for each ensemble member and simulation site based on climate and growing degree days (GDD) requirements. We calculated GDD for each simulation site through accumulated heat units starting from February 1st with a base temperature of 8°C (Kim et al., 2012) and determined the planting date once GDD surpassed the sampled for each ensemble member (Table 2, *gdd*). This led to earlier planting dates in warmer regions and vice versa (Fig. 7), and created diversity in cropping cycle start time among  $T \times M$  combinations, mimicking early versus late-planting cultivars (Fig. 13). To simulate well-fertilized conditions, we prescribed a total of 200 kg  $\text{ha}^{-1}$  of nitrogen throughout the growing season, applying half as base fertilizer prior to planting and the rest top-dressed one month post planting.

For each simulation site, we ran the MAZSIM model with default parameters that represented a generic crop cultivar across all locations (see default values in Table 2). Next, we carried out a site-level ensemble of simulations in which we used past meteorology data (see section 2.2) to each of the 100 trait-management parameter combinations (see section 2.5) for each of our 1160 site-years (see section 2.6) and identified top performing (high yield and yield stability) trait-management combinations. Finally, we repeated the site-specific trait and management ensemble of simulations with idealized future climate (see section 2.3) to understand how high performing trait and management combinations under current climate conditions fared under future climate.

## 2.10 Model validation

We validated simulated yields with default parameter values (control  $T \times M$  combination, see Table 2) with historic yield data from the United States Department of Agriculture – National Agriculture Statistics Service (USDA- NASS, [https://www.nass.usda.gov/Data\\_and\\_Statistics/index.php](https://www.nass.usda.gov/Data_and_Statistics/index.php)). We compared yield

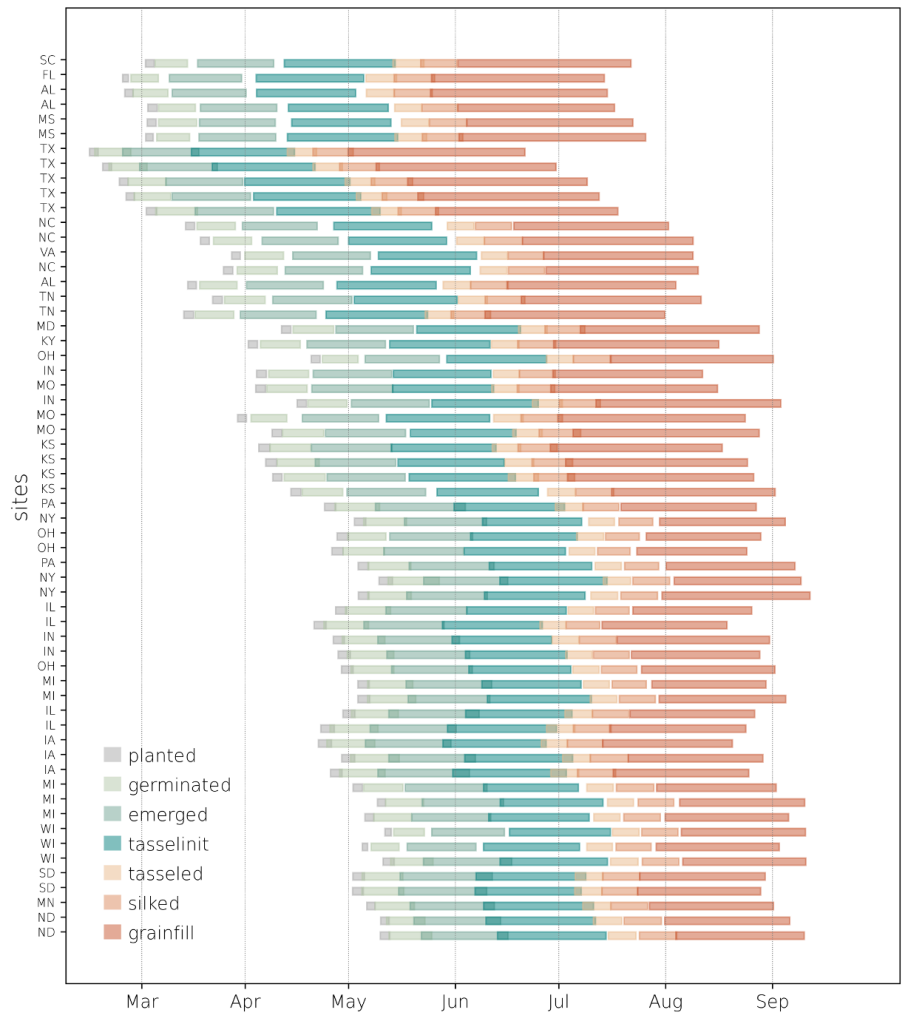


Figure 7: Start time and duration of each phenological stage across simulation sites, indicated by state abbreviations. Sites are roughly ranked by latitude, starting from southernmost sites towards the top.

data from observation sites closest to our simulation sites calculated through a Euclidean distance (Fig. 8). We scaled our whole-plant level simulation outputs to field level by applying a planting density of 10 plants per  $\text{m}^2$  and compared our simulated yield with averaged yield observations in between years 2005-2012, since our default parameter and management options resemble modern-day plant traits, planting density, and planting dates.

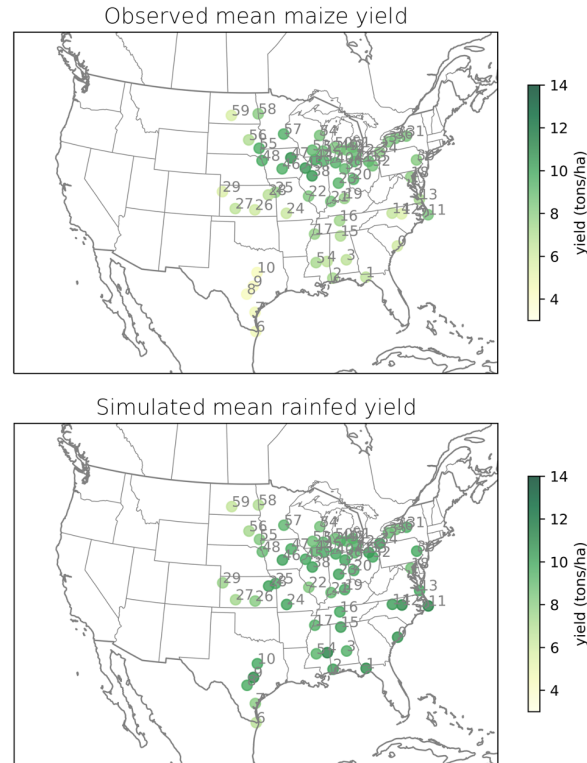


Figure 8: Observed (top) and simulated (bottom) yield (tons/ha) across simulated sites. Numbers indicate site numbers that correspond in Fig. 9.

### 3 Results and discussion

#### 3.1 Model validation

In general, simulated yields showed less spatial difference compared to observations (Fig. 8). The model captured historic yield observations well in the higher latitude Corn Belt regions but overestimated yield in various warmer sites in southern locations (Fig. 9). Southern locations experience much warmer temperatures, especially during later parts of the growing season (Fig. S3,

grain-fill). While MAZSIM dynamically describes temperature and water stress throughout the growing season through impacts on gas exchange and leaf developmental processes, the model lacks direct depiction of climate stress responses on reproduction processes such as flowering, pollination, and grain-filling, which are likely reasons for the yield over-estimation in warmer regions.

Cultivar differences between crops planted in southern versus northern locations could also contribute to these discrepancies. Farmers in warmer southern locations choose cultivars that are both planted and harvested earlier in the growing season, leading to an overall shorter crop cycle duration compared to those planted in the north (USDA-NASS, Crop Progress and Conditions). While our simulation set up captures earlier planting in warmer regions (Fig. 7), it does not capture potential differences in cultivar and management choices that growers in the south have likely been opting for in order to avoid late season heat and water stress. Finally, we note that by applying a universal soil depth (200 cm), we may be overestimating soil water availability. This could disproportionately affect warmer locations in south, in which late-season water availability could partially alleviate water stress later in the growing season and contribute to yield overestimation in those locations (Fig. 9).

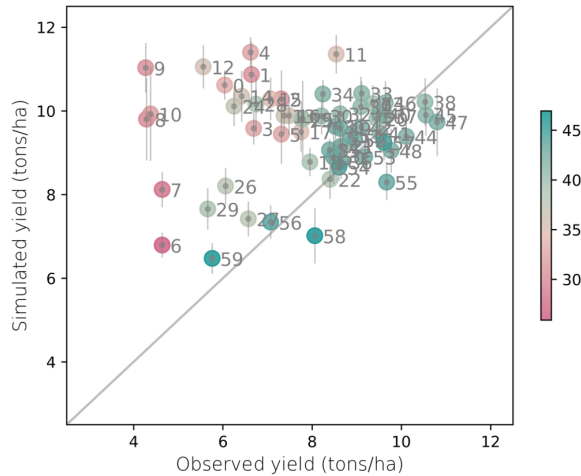


Figure 9: Observed versus simulated yield (tons/ha) across simulated sites. Colors indicate latitude of simulation site. Numbers correspond to site numbers shown in Fig. 8.

### 3.2 Performance difference across climate spaces

In Hsiao et al. (2022, submitted), we followed the framework described in this paper and identified several top-performing strategies among all  $T \times M$  combinations under present-day and future climate conditions, categorized based



on different combinations of phenological (grain-filling start time and duration) and morphological (total leaf area) features. Top-performing strategies under present-day climate conditions included  $T \times M$  combinations that either reached reproductive stage early (*Early Starting*), were slow in aging (*Slow Aging*), stress averting (*Stress Averting*), or had large canopies and were high in yielding (*High Yielding*). More details are described in Hsiao et al. (2022) and briefly summarized below.

*Early Starting*, *Slow Aging*, and *Stress Averting* strategies all have a smaller canopy size and relatively earlier transition times from vegetative to reproductive stages, but differ in grain-filling duration. *Slow Aging* strategies have long grain-filling durations that prolong cropping duration, while *Stress Averting* strategies display the shortest longevity, allowing plants with this strategy to complete their cropping cycle early and avoid late season stressors such as dry and hot conditions. On the other hand, *High Yielding* strategies have larger canopy sizes accompanied by delayed transition from vegetative to reproductive stages. While all categorized as top-performing under present-day climate, these strategies showcase a range of trade-offs between yield and yield stability, with performance differing across simulation sites (Fig. 5, 10) and climate spaces (Fig. 11a).

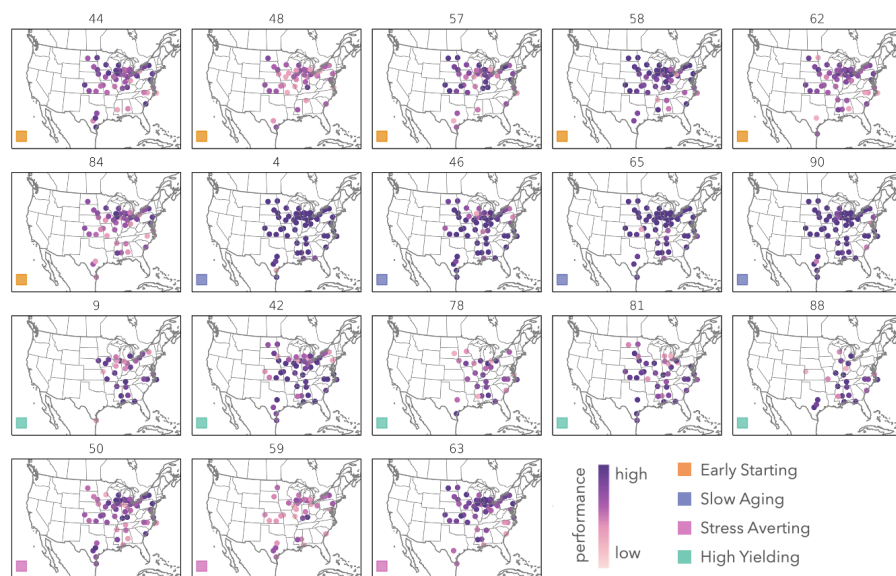


Figure 10: Performance ranking across simulation sites for  $T \times M$  combinations of different top-performing strategies under present-day climate conditions.

Under current climate conditions,  $T \times M$  combinations with *Slow Aging* strategies tend to be generalists, showing high performance across all climate spaces. On the other hand, strategies such as *Early Starting* fared best in cool

and wet regions, while *High Yielding* strategies perform best under warm and wet conditions (Fig. 11a). Under future climate conditions, we observed an overall yield loss for all  $T \times M$  combinations in most simulation sites (Fig. 12), including strategies that improved in performance ranking with climate change (Fig. 12a), such as *High Yielding* and *Large Canopy* (Fig. 11c). In general, warmer regions with low precipitation levels exhibited the greatest yield sensitivity (% yield loss per degree C of warming, Fig. 12); high-performing strategies under future climate partially buffered, but did not prevent yield loss.

High-performing strategies under present-day climate conditions shifted with climate change (Fig. 11b, c).  $T \times M$  combinations with early starting strategies experienced the greatest drop in performance ranking overall, showing declines in most climate spaces (Fig. 11c, *Early Starting*). Slow aging strategies still remained one of the higher performers by the end of the century (Fig. 11b, *Slow Aging*), but showed clear performance ranking declines in warm climate spaces (Fig. 11c, *Slow Aging*), allowing several other strategies to compete for top performance in those climate spaces (Fig. 11c);  $T \times M$  combinations with high yielding and compensating strategies progressed further in performance ranking (Fig. 11c, *High Yielding*), and new high-performing strategies with larger canopies and delayed transition timings into reproductive stages emerged (Fig. 11c, *Large Canopy*, *Compensating*, *Middle Ground*).

### 3.3 Mechanisms for high performance

We analyzed detailed in-season outputs of various phenological, physiological, and morphological outputs of the model (Table 3) and describe here some general trends observed in top-performing  $T \times M$  combinations.

#### 3.3.1 Phenology

Climatological differences between simulation sites and parameter differences among  $T \times M$  combinations both lead to the range of phenology output we see in our simulation outputs (Fig. 7, 13). Phenology differs across simulation sites due to imposed planting date adjustments based on growing degree day requirements, allowing for an earlier planting date in warmer regions (Fig. 7). Climatological differences throughout the growing season further shape the difference, especially during the grain-filling stage in which simulation sites in the south become substantially warmer than those in the north (Fig. S3), leading to hastened development (Fig. S5). On the other hand, phenology differs among  $T \times M$  combinations due to differences in perturbed traits linked to phenology (e.g. planting time, developmental rate, leaf number, Fig. 13). High performing  $T \times M$  combinations under present-day climate conditions tend to show earlier starts in reproductive stages with a longer duration (Fig. 13). Higher ranking  $T \times M$  combinations tend to show a greater fraction of grain-filling length over total growing season length (Fig. S4b) despite no clear trends in total growing season length (Fig. S4a).

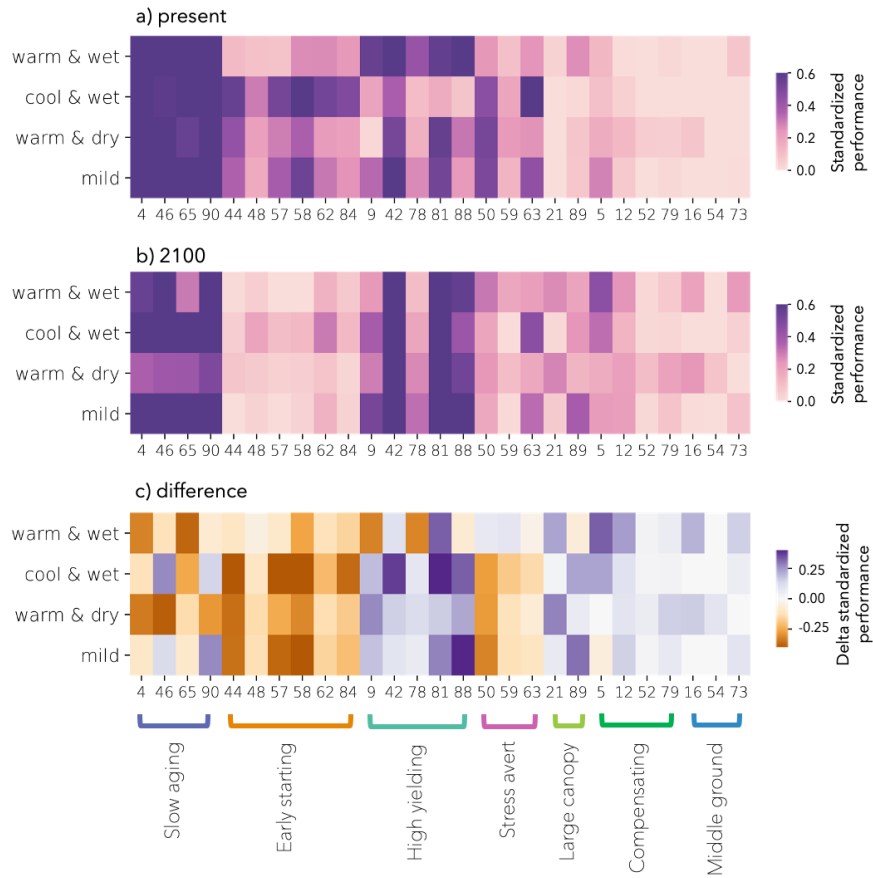


Figure 11: Standardized performance rankings of different strategies across climate spaces (see section 2.7) under a) current, b) future climate conditions, and c) the difference between the two.

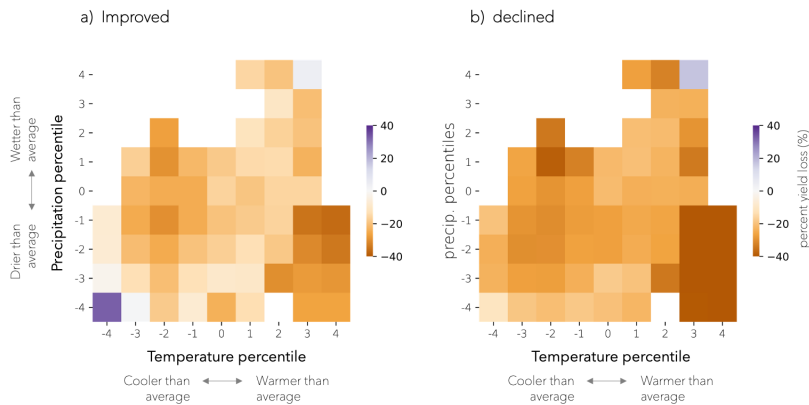


Figure 12: Percent yield loss within mean growing season temperature-precipitation climate space among  $T \times M$  combinations that a) improved versus, b) declined in performance ranking under future climate conditions.

### 3.3.2 Physiology

Net photosynthetic rates are generally higher in top-performing  $T \times M$  combinations during transition from vegetative into reproductive stages (Fig. S6), but the differences in photosynthetic rates become dominated by climatological differences between simulation sites during the final grain-filling stage, with greater photosynthetic rates in warmer southern regions (Fig. S6). In general, we see a linear relationship between temperature and photosynthetic rate during vegetative stages (Fig. 14). This relationship eventually plateaus around 28-30 °C later in the growing season, and starts to decline in a few warmest site-years (Fig. 14b). While warmer temperatures generally led to higher photosynthetic rates, hastened development and greater water deficit under warmer conditions also led to overall shorter grain-filling durations (Fig. S7, S5a), compensating one another, dampening the overall difference between northern versus southern sites in terms of net carbon gained throughout grain-filling (Fig. S8) and final yield (Fig. S9).

### 3.3.3 Morphology

Differences in simulated total leaf area was largely dominated by parameter make up within  $T \times M$  combinations, showing much less difference in simulated yield across sites (Fig. S10). Simulated plants approached full canopy sizes around tassel initiation, and top-performing combinations showed mid to lower total leaf area under present-day climate conditions. This was consistent with most top-performers under present-day climate exhibiting early transitions into reproductive stage (e.g., *Slow Aging*, *Early Starting*, *Stress Averting*). These strategies partly achieved early reproductive start through short vegetative stages through fewer total number of leaves and hence smaller canopy size (i.e., lower

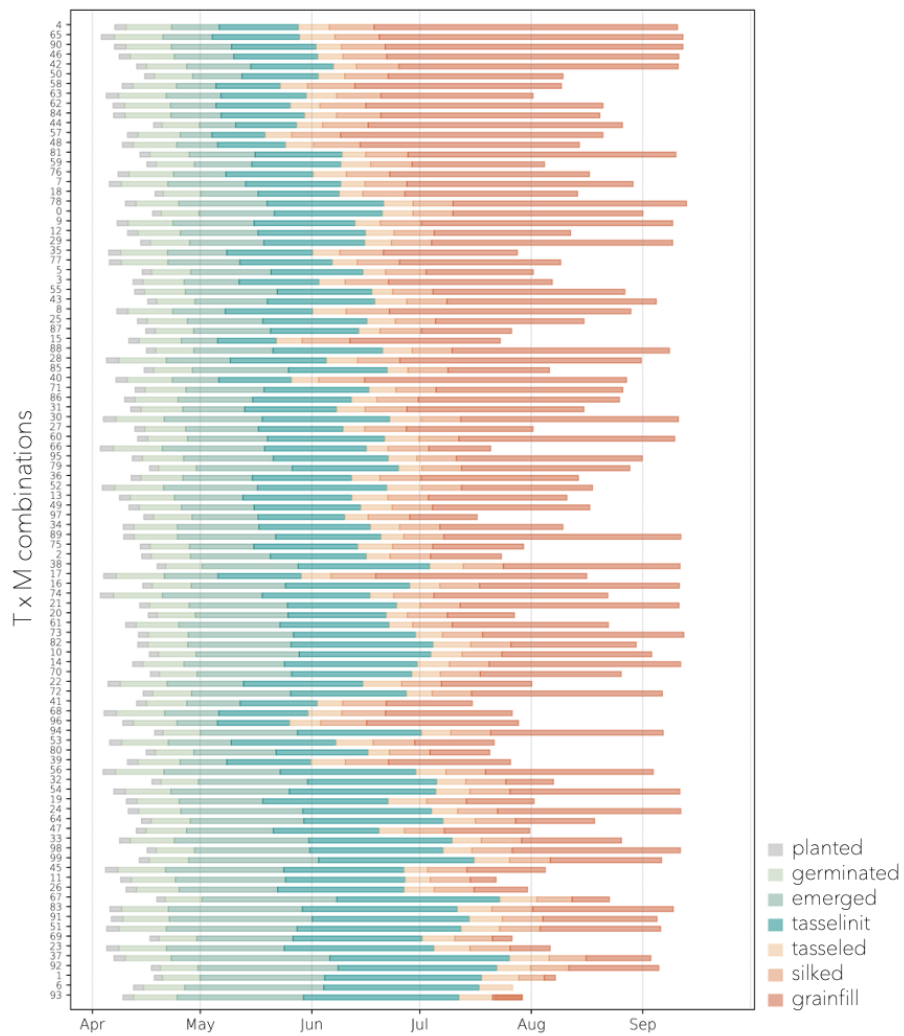


Figure 13: Start time and duration of each phenological stage across  $T \times M$  combinations, averaged across all simulation sites, ranked by overall performance, with the highest performers listed towards the top.

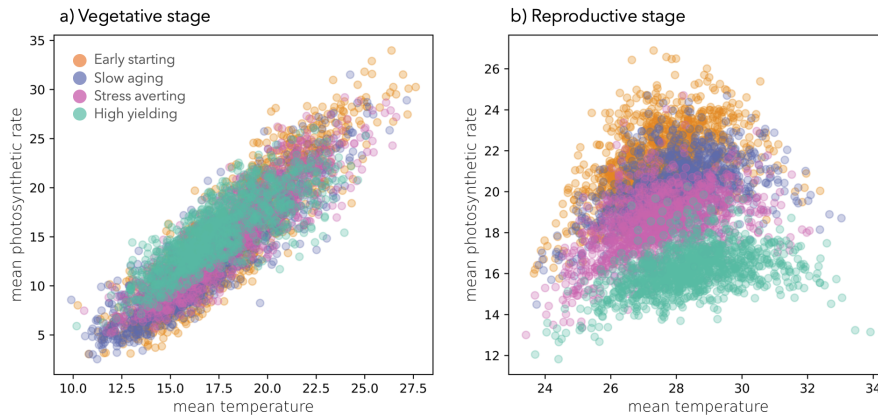


Figure 14: Relationship between mean temperature ( $^{\circ}\text{C}$ ) and mean photosynthetic rate ( $\mu\text{mol CO}_2 \text{ m}^{-2} \text{ sec}^{-1}$ ) for all simulated site-years during a) vegetative versus b) reproductive stages for four representative  $T \times M$  combinations within top-performing strategies.

total leaf area).

## 4 Discussion

Crop production is expected to suffer under future climate conditions as the climate warms. Adaptation of crop management practices, location of planting, as well as adaptation of the crops themselves all have the potential to limit expected yield loss and help to sustain agricultural productivity. However, we lack a systematic understanding of which adaptations are likely to have the biggest impact and why, both critical pieces of knowledge for agricultural planning. Mechanistic, process-based crop simulation models can be a powerful tool to synthesize cropping information, set breeding targets, and develop adaptation strategies for sustaining food production, yet have been underutilized for developing specific climate-adaptation options.

Breeding for and adopting new cultivars involve exploring and navigating the hills and valleys of the  $G \times E \times M$  landscape, in which optimal plant traits and management options are identified within defined target environments (Cooper et al., 2016; Messina et al., 2011). Requirements from breeding, delivering, and adopting a desirable cultivar depends on many factors, and the whole process can take from years to decades (Challinor et al., 2017). Recent developments in breeding practices have greatly expanded the efficiency in genotyping and phenotyping methods (Voss-Fels et al., 2019), yet the breeding pipeline is still time and resource intensive, limiting its ability to explore the full range of  $G \times E \times M$  combinations and interactions.

A typical breeding cycle starts out by exposing a large germplasm pool under

extremely high selection pressure, filtering genotypes from the order of  $10^6$  individuals down to a few dozen promising candidates (Cooper et al., 2014; Messina, Cooper, Hammer, et al., 2020). In the early stages of a breeding program, trait selection is often limited to those that can easily be identified through automated processes, and commonly based on plants in early developmental stages. It is not until later in the breeding cycle that selection criteria shift from genotype to phenotype-based, and promising hybrids are evaluated on-farm at various locations with a range of background climate conditions (Gaffney et al., 2015). Management optimization also occurs around this time, in which field trials are set up to identify the best management practices for the final candidates prior to commercial release. Further, common breeding methods that either select for higher yield or eliminate defect traits do not allow for a clear understanding of the mechanisms in which favorable traits contribute to greater performance and yield, and effective combinations of plant traits, if not actively sought for based on a mechanistic understanding of crop growth and yield, could only occur by chance (Donald, 1968).

There is growing recognition that mechanistic crop simulation models can be a powerful tool to synthesize cropping information, set breeding targets, and develop adaptation strategies for sustaining food production. Such applications can complement current breeding efforts of developing new climate-resilient cultivars by facilitating broad exploration of the  $G \times E \times M$  landscape within a modeled setting as a first step (Cooper et al., 2020; Messina, Cooper, Reynolds, et al., 2020; Muller & Martre, 2019; Rötter et al., 2015). The process-based nature of such models allow for mechanistic insight through which these adaptations influence yield and their sensitivity to different climate factors, providing a more complete assessment of the uncertainty associated with different possible climate conditions, including those that do not currently exist yet.

Ramirez-Villegas et al. (2015) provided a few successful examples of model-aided breeding projects, such as the New Plant Type program developed by IRRI for rice crops, in which process-based models were used to help make informed decisions to target breeding directions and resulted in new plant types that out-yielded conventional cultivars within two breeding cycles (S. Peng et al., 2008). This success further inspired the super rice program in China that led to newly developed rice varieties with 15-25% higher yield than common hybrid cultivars planted in other regions in China (S. Peng et al., 2008). While model-aided breeding practices are less commonly targeted towards a changing climate (Ramirez-Villegas et al., 2015), demonstrated success under current climate suggest it as a promising pathway to guide breeding direction for climate adaptation moving forward, and expanded experiments evaluating a range of  $G \times E \times M$  conditions can enable production system responses to changing environmental conditions (Messina et al., 2020, Wang et al., 2019).

Regardless, thorough evaluation and application of crop models for developing specific climate-adaptation options (e.g., designing adaptive phenotypes for specific soil-climate combinations) for US agriculture remains scarce. We bridge this gap by constructing an integrated data-model framework set up to explore crop performance across a defined  $G \times E \times M$  landscape. With this framework,

we identified high-performing plant trait and management combinations ( $G \times M$ ) best suited for current climate conditions, as well as targets and priorities to adapt to impending climate stressors (E). Heterogeneity in performance exists within the sampled climate space, which stemmed from underlying physiological, morphological, and phenological processes within the simulated crop. Model outputs on hourly time steps allowed us to compile detailed in-season outputs of various plant processes and summarize them according to associated phenological stages. This form of model output allows for more in-depth analysis that go beyond final yield and yield stability, and investigation of mechanisms that contribute to high crop performance and the differences across climate spaces and under future climate projections.

We demonstrate how such a framework can be used to identify adaptation options with an emphasis on climate-resilient plant traits and effective management that will mitigate yield loss and optimize productivity both across space and through time in US corn growing regions under future climate conditions. Our modeling results demonstrate that application of mechanistic modeling holds substantial promise to inform breeding within the US maize production system.

## 5 Acknowledgements

We thank Lucas Vargas Zeppetello for providing CMIP6 temperature and relative humidity projection scaling patterns. JH acknowledges support from the AFRI NIFA Fellowships Grant Program: Predoctoral Fellowships [grant no. 2020-67034-31736] from the USDA National Institute of Food and Agriculture. ALSS acknowledges support from NSF AGS-1553715.



## References

- Andrивon, D., Giorgetti, C., Baranger, A., Calonnec, A., Cartolaro, P., Faivre, R., Guyader, S., Lauri, P. E., Lescourret, F., Parisi, L., Ney, B., Tivoli, B., & Sache, I. (2012). Defining and designing plant architectural ideotypes to control epidemics ? *Eur J Plant Patol.* <https://doi.org/10.1007/s10658-012-0126-y>
- Ball, J. T., Woodrow, I. E., & Berry, J. A. (1987). A model predicting stomatal conductance and its contribution to the control of photosynthesis under different environmental conditions. *Progress in photosynthesis research*, 4(5), 221–224. [https://doi.org/10.1007/978-94-017-0519-6\\_48](https://doi.org/10.1007/978-94-017-0519-6_48)
- Bassu, S., Brisson, N., Durand, J.-L., Boote, K., Lizaso, J., Jones, J. W., Rosenzweig, C., Ruane, A. C., Adam, M., Baron, C., Basso, B., Biernath, C., Boogaard, H., Conijn, S., Corbeels, M., Deryng, D., Sanctis, G. D., Gayler, S., Grassini, P., ... Waha, K. (2014). How do various maize crop models vary in their responses to climate change factors? *Global Change Biology*, 20(7), 2301–2320.
- Burke, M. B., Lobell, D. B., & Guarino, L. (2009). Shifts in African crop climates by 2050 , and the implications for crop improvement and genetic resources conservation. *Global Environmetnal Change*, 19, 317–325. <https://doi.org/10.1016/j.gloenvcha.2009.04.003>
- Butler, E. E., Mueller, N. D., & Huybers, P. (2018). Peculiarly pleasant weather for US maize. *Proceedings of the National Academy of Sciences of the United States of America*, 115(47), 11935–11940. <https://doi.org/10.1073/pnas.1808035115>
- Campbell, G. S. (1986). *Extinction coefficients for radiation in plant canopies calculated using an ellipsoidal inclination angle distribution* (tech. rep.).
- Cardwell, V. B. (1982). Fifty Years of Minnesota Corn Production: Sources of Yield Increase1. *Agronomy Journal*, 74(6), 984. <https://doi.org/10.2134/agronj1982.00021962007400060013x>
- Challinor, A. J., Müller, C., Asseng, S., Deva, C., Nicklin, K. J., Wallach, D., Vanuytrecht, E., Whitfield, S., Ramirez-Villegas, J., & Koehler, A. K. (2017). Improving the use of crop models for risk assessment and climate change adaptation. *Agricultural Systems*, 159, 296–306. <https://doi.org/10.1016/j.agry.2017.07.010>
- Collatz, G. J., Ribas-Carbo, M., & Berry, J. A. (1992). Coupled Photosynthesis-Stomatal Conductance Model for Leaves of C4 Plants. *Australian Journal of Plant Physiology*, 19(5), 519–538. <https://doi.org/10.1071/PP9920519>
- Cooper, M., Messina, C. D., Podlich, D., Totir, L. R., Baumgarten, A., Hausmann, N. J., Wright, D., & Graham, G. (2014). Predicting the future of plant breeding: Complementing empirical evaluation with genetic prediction. *Crop and Pasture Science*, 65(4), 311–336. <https://doi.org/10.1071/CP14007>
- Cooper, M., Tang, T., Gho, C., Hart, T., Hammer, G., & Messina, C. (2020). Integrating genetic gain and gap analysis to predict improvements in

- crop productivity. *Crop Science*, *60*(2), 582–604. <https://doi.org/10.1002/csc2.20109>
- Cooper, M., Technow, F., Messina, C., Gho, C., & Radu Totir, L. (2016). Use of crop growth models with whole-genome prediction: Application to a maize multienvironment trial. *Crop Science*, *56*(5), 2141–2156. <https://doi.org/10.2135/cropsci2015.08.0512>
- de Pury, D. G. G., & Farquhar, G. D. (1997). Simple scaling of photosynthesis from leaves to canopies without the errors of big-leaf models. *Plant, Cell & Environment*, *20*, 537–557.
- Deryng, D., Sacks, W. J., Barford, C. C., & Ramankutty, N. (2011). Simulating the effects of climate and agricultural management practices on global crop yield. *Global Biogeochemical Cycles*, *25*(2). <https://doi.org/10.1029/2009gb003765>
- Donald, C. M. (1968). The breeding of crop ideotypes. *Euphytica*, *17*, 385–403.
- Donat, M. G., Pitman, A. J., & Seneviratne, S. I. (2017). Regional warming of hot extremes accelerated by surface energy fluxes. *Geophysical Research Letters*, *44*(13), 7011–7019. <https://doi.org/10.1002/2017GL073733>
- Durand, J.-L., Delusca, K., Boote, K., Lizaso, J., Manderscheid, R., Weigel, H. J., Ruane, A. C., Rosenzweig, C., Jones, J., Ahuja, L., Anapalli, S., Basso, B., Baron, C., Bertuzzi, P., Biernath, C., Deryng, D., Ewert, F., Gaiser, T., Gayler, S., . . . Zhao, Z. (2018). How accurately do maize crop models simulate the interactions of atmospheric CO<sub>2</sub> concentration levels with limited water supply on water use and yield? *Eur J Agron*, *100*, 67–75.
- Duvick, D. N. (2005). The Contribution of Breeding to Yield Advances in maize (*Zea mays* L.) [https://doi.org/10.1016/S0065-2113\(05\)86002-X](https://doi.org/10.1016/S0065-2113(05)86002-X)
- Dziewit, M. J., Li, X., & Yu, J. (2019). Dissection of Leaf Angle Variation in Maize through Genetic Mapping and Meta-Analysis. *The Plant Genome*, *12*(1), 180024. <https://doi.org/10.3835/plantgenome2018.05.0024>
- Fischer, R. A., & Edmeades, G. O. (2010). Breeding and cereal yield progress. *Crop Science*, *50*, S-85–S-98. <https://doi.org/10.2135/cropsci2009.10.0564>
- Fita, A., Rodríguez-Burruezo, A., Boscaiu, M., Prohens, J., & Vicente, O. (2015). Breeding and domesticating crops adapted to drought and salinity: A new paradigm for increasing food production. *Frontiers in Plant Science*, *6*, 1–14. <https://doi.org/10.3389/fpls.2015.00978>
- Gaffney, J., Schussler, J., Löffler, C., Cai, W., Paszkiewicz, S., Messina, C., Groeteke, J., Keaschall, J., & Cooper, M. (2015). Industry-scale evaluation of maize hybrids selected for increased yield in drought-stress conditions of the US corn belt. *Crop Science*, *55*(4), 1608–1618. <https://doi.org/10.2135/cropsci2014.09.0654>
- Godfray, H. C. J., Beddington, J. R., Crute, I. R., Haddad, L., Lawrence, D., Muir, J. F., Pretty, J., Robinson, S., Thomas, S. M., & Toulmin, C. (2010). Food Security: The Challenge of Feeding 9 Billion People. *Science*, *327*(5967), 812–818. <https://doi.org/10.1126/science.1185383>

- Gregersen, P. L., Culetic, A., Boschian, L., & Krupinska, K. (2013). Plant senescence and crop productivity. *Plant Molecular Biology*, *82*(6), 603–622. <https://doi.org/10.1007/s11103-013-0013-8>
- Hammer, G., McLean, G., Oosterom, E., Chapman, S., Zheng, B., Wu, A., Doherty, A., & Jordan, D. (2020). Designing crops for adaptation to the drought and high temperature risks anticipated in future climates. *Crop Science*, 1–17. <https://doi.org/10.1002/csc2.20110>
- Hammer, G. L., Dong, Z., McLean, G., Doherty, A., Messina, C., Schussler, J., Zinselmeier, C., Paszkiewicz, S., & Cooper, M. (2009). Can changes in canopy and/or root system architecture explain historical maize yield trends in the U.S. corn belt? *Crop Science*, *49*(1), 299–312. <https://doi.org/10.2135/cropsci2008.03.0152>
- Hatfield, J. L., & Walthall, C. L. (2015). Meeting Global Food Needs : Realizing the Potential via Genetics  $\times$  Environment  $\times$  Management Interactions, 1215–1226. <https://doi.org/10.2134/agronj15.0076>
- Hsiao, J., Kim, S.-H., Timlin, D. J., Mueller, N. D., & Swann, A. L. S. (2022). Model-aided climate adaptation for future maize in the u.s. *submitted*.
- Hsiao, J., Swann, A. L. S., & Kim, S.-H. (2019). Maize yield under a changing climate: The hidden role of vapor pressure deficit. *Agricultural and Forest Meteorology*, *279*, 107692. <https://doi.org/10.1016/j.agrformet.2019.107692>
- Kim, S.-H., Sicher, R. C., Bae, H., Gitz, D. C., Baker, J. T., Timlin, D. J., & Reddy, V. R. (2006). Canopy photosynthesis, evapotranspiration, leaf nitrogen, and transcription profiles of maize in response to CO<sub>2</sub> enrichment. *Global Change Biology*, *12*(3), 588–600. <https://doi.org/10.1111/j.1365-2486.2006.01110.x>
- Kim, S.-H., Yang, Y., Timlin, D. J., Fleisher, D. H., Dathe, A., Reddy, V. R., & Staver, K. (2012). Modeling temperature responses of leaf growth, development, and biomass in maize with MAZSIM. *Agronomy Journal*, *104*(6), 1523–1537. <https://doi.org/10.2134/agronj2011.0321>
- Kimball, B. A., Boote, K. J., Hatfield, J. L., Ahuja, L. R., Stockle, C., Archontoulis, S., Baron, C., Basso, B., Bertuzzi, P., Constantin, J., Deryng, D., Dumont, B., Durand, J. L., Ewert, F., Gaiser, T., Gayler, S., Hoffmann, M. P., Jiang, Q., Kim, S. H., . . . Williams, K. (2019). Simulation of maize evapotranspiration: An inter-comparison among 29 maize models. *Agricultural and Forest Meteorology*, *271*, 264–284. <https://doi.org/10.1016/j.agrformet.2019.02.037>
- Kucharik, C. J. (2008). Contribution of planting date trends to increased maize yields in the central United States. *Agronomy Journal*, *100*(2), 328–336. <https://doi.org/10.2134/agronj2007.0145>
- Lizaso, J. I., Batchelor, W. D., & Westgate, M. E. (2003). A leaf area model to simulate cultivar-specific expansion and senescence of maize leaves. *Field Crops Research*, *80*(1), 1–17. [https://doi.org/10.1016/S0378-4290\(02\)00151-X](https://doi.org/10.1016/S0378-4290(02)00151-X)
- McCouch, S., Baute, G. J., Bradeen, J., Bramel, P., Bretting, P. K., Buckler, E., Burke, J. M., Charest, D., Cloutier, S., Cole, G., Dempewolf, H.,

- Dingkuhn, M., Feuillet, C., Gepts, P., Grattapaglia, D., Guarino, L., Jackson, S., Knapp, S., Langridge, P., ... Zamir, D. (2013). Feeding the future. *Nature*, *499*(7456), 23–24. <https://doi.org/10.1038/499023a>
- McKay, M. D., Beckman, R. J., & Conover, W. J. (1979). A comparison of three methods for selecting values of input variables in the analysis of output from a computer code. *Technometrics*, *21*(2), 239–245. <https://doi.org/10.1080/00401706.2000.10485979>
- Messina, C. D., Cooper, M., Hammer, G. L., Berning, D., Ciampitti, I., Clark, R., Diepenbrock, C., Gho, C., Jines, M., Lee, T., McCormick, R., Mihura, E., Podlich, D., Rotundo, J., Smalley, M., Tang, T., Truong, S., & van Eeuwijk, F. (2020). Two decades of creating drought tolerant maize and underpinning prediction technologies in the US corn-belt: Review and perspectives on the future of crop design. *bioRxiv*. <https://doi.org/10.1101/2020.10.29.361337>
- Messina, C. D., Cooper, M., Reynolds, M., & Hammer, G. L. (2020). Crop science: A foundation for advancing predictive agriculture. *Crop Science*, *60*(2), 544–546. <https://doi.org/10.1002/csc2.20116>
- Messina, C. D., Podlich, D., Dong, Z., Samples, M., & Cooper, M. (2011). Yield-trait performance landscapes: From theory to application in breeding maize for drought tolerance. *Journal of Experimental Botany*, *62*(3), 855–868. <https://doi.org/10.1093/jxb/erq329>
- Messina, C. D., Sinclair, T. R., Hammer, G. L., Curan, D., Thompson, J., Oler, Z., Gho, C., & Cooper, M. (2015). Limited-transpiration trait may increase maize drought tolerance in the US corn belt. *Agronomy Journal*, *107*(6), 1978–1986. <https://doi.org/10.2134/agronj15.0016>
- Miner, G. L., Bauerle, W. L., & Baldocchi, D. D. (2017). Estimating the sensitivity of stomatal conductance to photosynthesis: a review. *Plant Cell and Environment*, *40*(7), 1214–1238. <https://doi.org/10.1111/pce.12871>
- Mueller, N. D., Butler, E. E., McKinnon, K. A., & Rhines, A. (2016). Cooling of US Midwest summer temperature extremes from cropland intensification. *Nature Climate Change*, *6*(3). <https://doi.org/10.1038/nclimate2825>
- Muller, B., & Martre, P. (2019). Plant and crop simulation models: Powerful tools to link physiology, genetics, and phenomics. *Journal of Experimental Botany*, *70*(9), 2339–2344. <https://doi.org/10.1093/jxb/erz175>
- O'Neill, B. C., Tebaldi, C., Van Vuuren, D. P., Eyring, V., Friedlingstein, P., Hurtt, G., Knutti, R., Kriegler, E., Lamarque, J. F., Lowe, J., Meehl, G. A., Moss, R., Riahi, K., & Sanderson, B. M. (2016). The Scenario Model Intercomparison Project (ScenarioMIP) for CMIP6. *Geoscientific Model Development*, *9*(9), 3461–3482. <https://doi.org/10.5194/gmd-9-3461-2016>
- Padilla, J. M., & Otegui, M. E. (2005). Co-ordination between leaf initiation and leaf appearance in field-grown maize (*Zea mays*): Genotypic differences in response of rates to temperature. *Annals of Botany*, *96*(6), 997–1007. <https://doi.org/10.1093/aob/mci251>
- Parent, B., Leclere, M., Lacube, S., Semenov, M. A., Welcker, C., Martre, P., & Tardieu, F. (2018). Maize yields over Europe may increase in spite

- of climate change, with an appropriate use of the genetic variability of flowering time. *Proceedings of the National Academy of Sciences of the United States of America*, *115*(42), 10642–10647. <https://doi.org/10.1073/pnas.1720716115>
- Peng, B., Guan, K., Tang, J., Ainsworth, E. A., Asseng, S., Bernacchi, C. J., Cooper, M., Delucia, E. H., Elliott, J. W., Ewert, F., Grant, R. F., Gustafson, D. I., Hammer, G. L., Jin, Z., Jones, J. W., Kimm, H., Lawrence, D. M., Li, Y., Lombardozzi, D. L., . . . Zhou, W. (2020). Towards a multiscale crop modeling framework for climate change adaptation assessment. *Nature Plants*, *6*(April). <https://doi.org/10.1038/s41477-020-0625-3>
- Peng, S., Khush, G. S., Virk, P., Tang, Q., & Zou, Y. (2008). Progress in ideotype breeding to increase rice yield potential. *Field Crops Research*, *108*(1), 32–38. <https://doi.org/10.1016/j.fcr.2008.04.001>
- Ramirez-Villegas, J., Watson, J., & Challinor, A. J. (2015). Identifying traits for genotypic adaptation using crop models. *Journal of Experimental Botany*, *66*(12), 3451–3462. <https://doi.org/10.1093/jxb/erv014>
- Riahi, K., van Vuuren, D. P., Kriegler, E., Edmonds, J., O'Neill, B. C., Fujimori, S., Bauer, N., Calvin, K., Dellink, R., Fricko, O., Lutz, W., Popp, A., Cuaresma, J. C., KC, S., Leimbach, M., Jiang, L., Kram, T., Rao, S., Emmerling, J., . . . Tavoni, M. (2017). The Shared Socioeconomic Pathways and their energy, land use, and greenhouse gas emissions implications: An overview. *Global Environmental Change*, *42*, 153–168. <https://doi.org/10.1016/j.gloenvcha.2016.05.009>
- Rötter, R. P., Tao, F., Höhn, J. G., & Palosuo, T. (2015). Use of crop simulation modelling to aid ideotype design of future cereal cultivars. *Journal of Experimental Botany*, *66*(12), 3463–3476. <https://doi.org/10.1093/jxb/erv098>
- Sacks, W. J., & Kucharik, C. J. (2011). Crop management and phenology trends in the U.S. Corn Belt: Impacts on yields, evapotranspiration and energy balance. *Agric. For. Meteorol.*, *151*(7), 882–894. <https://doi.org/10.1016/j.agrformet.2011.02.010>
- Shekoofa, A., Sinclair, T. R., Messina, C. D., & Cooper, M. (2016). Variation among maize hybrids in response to high vapor pressure deficit at high temperatures. *Crop Science*, *56*(1), 392–396. <https://doi.org/10.2135/cropsci2015.02.0134>
- Soil Survey Staff, U. S. D. A., Natural Resources Conservation Service. (n.d.). Soil Survey Geographic (SSURGO) Database. [Available online. Accessed [09/15/2019].].
- Soltani, A., & Hoogenboom, G. (2003). Minimum data requirements for parameter estimation of stochastic weather generators. *Climate Research*, *25*(2), 109–119. <https://doi.org/10.3354/cr025109>
- Staff, S. S. (1999). *Soil taxonomy: A basic system of soil classification for making and interpreting soil surveys. 2nd edition. natural resources conservation service. u.s. department of agriculture handbook 436.*

- Stone, P. J., Pearson, A. J., Sorensen, I. B., & Rogers, B. T. (2000). Effect of row spacing and plant population on maize yield and quality. *Agronomy New Zealand*, *30*, 67–75.
- Timlin, D., Kim, S.-H., Fleisher, D., Wang, Z., & Reddy, V. R. (2019). Chapter 3 - Maize water use and yield in the solar corridor system: a simulation study. In C. L. Deichman & R. J. Kremer (Eds.), *The solar corridor crop system* (pp. 57–78). Academic Press. <https://doi.org/https://doi.org/10.1016/B978-0-12-814792-4.00003-6>
- Timlin, D., Pachepsky, Y. A., & Acock, B. (1996). A design for a modular, generic soil simulator to interface with plant models. *Agronomy Journal*, *88*(2), 162–169. <https://doi.org/10.2134/agronj1996.00021962008800020008x>
- Tuzet, A., Perrier, A., & Leuning, R. (2003). A coupled model of stomatal conductance, photosynthesis and transpiration. *Plant, Cell & Environment*, *26*(7), 1097–1116.
- van Genuchten, M. T. (1980). A Closed-form Equation for Predicting the Hydraulic Conductivity of Unsaturated Soils. *Soil Science Society of America Journal*, *44*(5), 892–898. <https://doi.org/https://doi.org/10.2136/sssaj1980.03615995004400050002x>
- Van Wart, J., Grassini, P., & Cassman, K. G. (2013). Impact of derived global weather data on simulated crop yields. *Global Change Biology*, *19*(12), 3822–3834. <https://doi.org/10.1111/gcb.12302>
- Vargas Zeppetello, L. R., Battisti, D. S., & Baker, M. B. (2019). The origin of soil moisture evaporation “regimes”. *Journal of Climate*, *32*(20), 6939–6960. <https://doi.org/10.1175/JCLI-D-19-0209.1>
- von Caemmerer, S. (2000). *Biochemical Models of Leaf Photosynthesis*. CSIRO Publishing.
- Voss-Fels, K. P., Stahl, A., & Hickey, L. T. (2019). Q&A: Modern crop breeding for future food security 07 Agricultural and Veterinary Sciences 0703 Crop and Pasture Production 06 Biological Sciences 0607 Plant Biology 06 Biological Sciences 0604 Genetics. *BMC Biology*, *17*(1), 1–7.
- Wu, A., Hammer, G. L., Doherty, A., von Caemmerer, S., & Farquhar, G. D. (2019). Quantifying impacts of enhancing photosynthesis on crop yield. *Nature plants*, *5*(4), 380–388. <https://doi.org/10.1038/s41477-019-0398-8>
- Yang, Y., Kim, S.-H., Timlin, D. J., Fleisher, D. H., Quebedeaux, B., & Reddy, V. R. (2009). Simulating canopy transpiration and photosynthesis of corn plants under contrasting water regimes using a coupled model. *Transactions of the ASABE*, *52*(3), 1011–1024. <https://doi.org/10.13031/2013.27370>
- Yang, Y., Timlin, D. J., Fleisher, D. H., Kim, S. .-, Quebedeaux, B., & Reddy, V. R. (2009). Simulating leaf area of corn plants at contrasting water status. *Agricultural and Forest Meteorology*, *149*(6-7), 1161–1167. <https://doi.org/10.1016/j.agrformet.2009.02.005>
- Yin, X., Kropff, M. J., McLaren, G., & Visperas, R. M. (1995). A nonlinear model for crop development as a function of temperature. *Agricultural*

- and Forest Meteorology*, 77(1-2), 1–16. [https://doi.org/10.1016/0168-1923\(95\)02236-Q](https://doi.org/10.1016/0168-1923(95)02236-Q)
- Zhang, J., Fengler, K. A., Van Hemert, J. L., Gupta, R., Mongar, N., Sun, J., Allen, W. B., Wang, Y., Weers, B., Mo, H., Lafitte, R., Hou, Z., Bryant, A., Ibraheem, F., Arp, J., Swaminathan, K., Moose, S. P., Li, B., & Shen, B. (2019). Identification and characterization of a novel stay-green QTL that increases yield in maize. *Plant Biotechnology Journal*, 17(12), 2272–2285. <https://doi.org/10.1111/pbi.13139>
- Zhu, P., Jin, Z., Zhuang, Q., Ciaia, P., Bernacchi, C., Wang, X., Makowski, D., & Lobell, D. (2018). The important but weakening maize yield benefit of grain filling prolongation in the US Midwest, 4718–4730. <https://doi.org/10.1111/gcb.14356>

## 6 Supplementary information

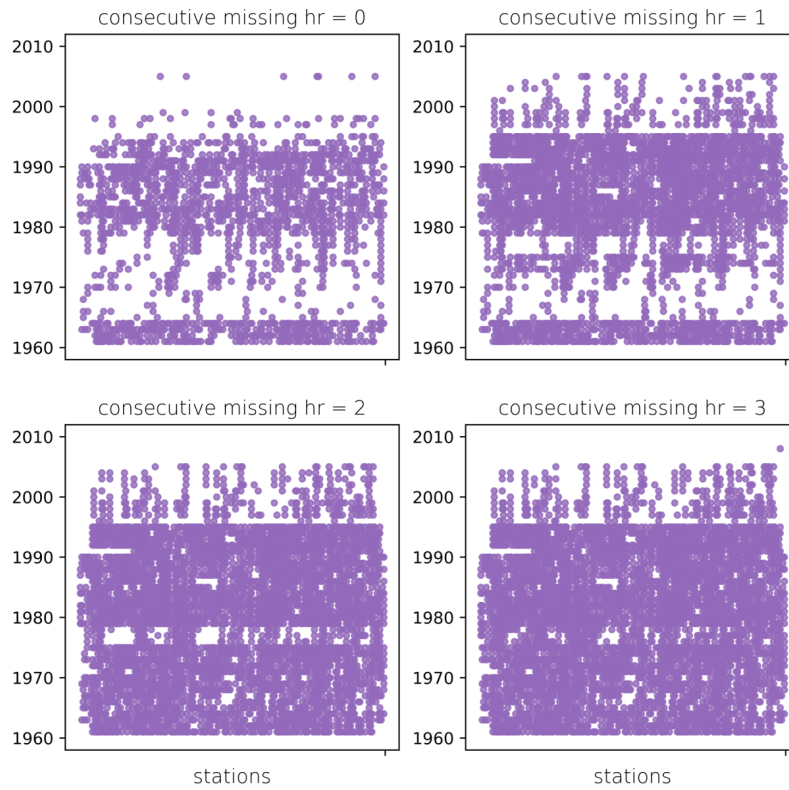


Figure S1: Available weather data based on different gap-filling intervals. For example, if consecutive missing hours equals 0, then only site-years with complete hourly weather data records will be included for weather data. If consecutive missing hour equals 1, site-years with gaps no greater than one hour consecutively will be included and gap-filled linearly.



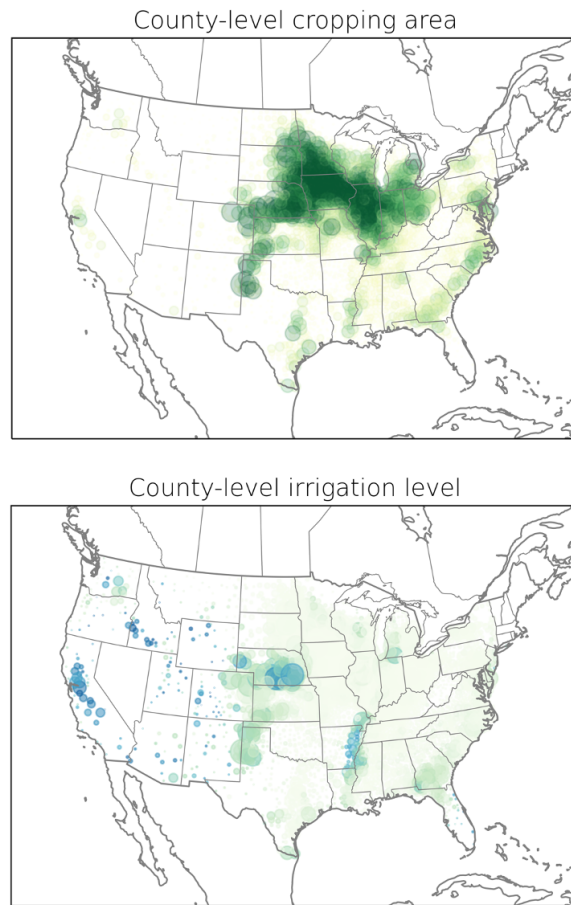


Figure S2: Maize planting area (top) and irrigation levels (bottom) across continental U.S.

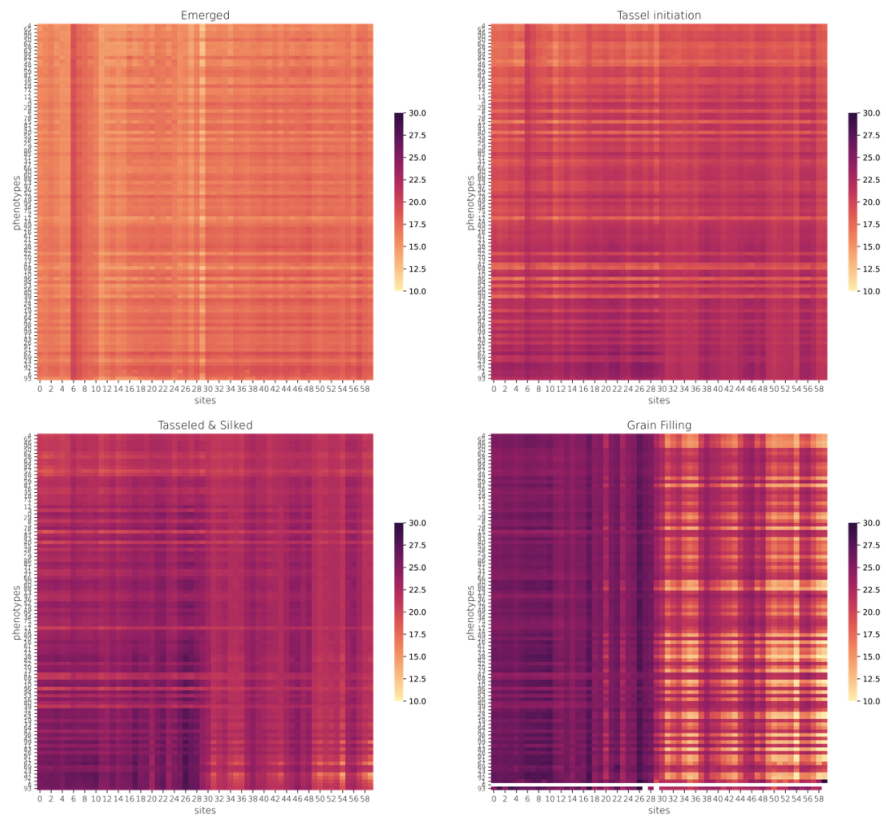


Figure S3: Mean air temperature ( $^{\circ}\text{C}$ ) across phenological stages for top phenotypes across all sites, ranked by performance of  $T \times M$  combinations, and averaged within phenological stages.

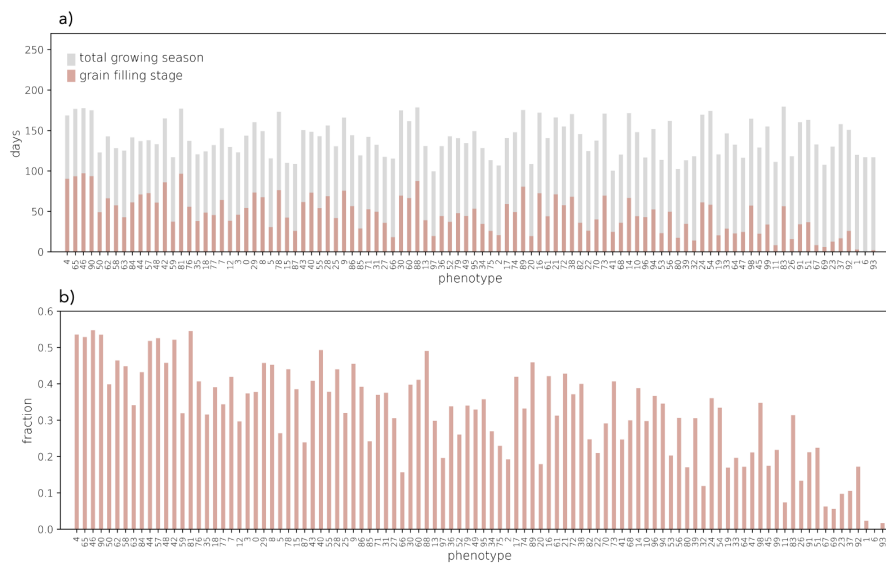


Figure S4: a) Total growing season length (gray, days) and grain-filling length (pink, days) for all phenotypes, ranked by performance, starting with the highest performers towards the left, and b) the fraction of grain-filling over total growing season.

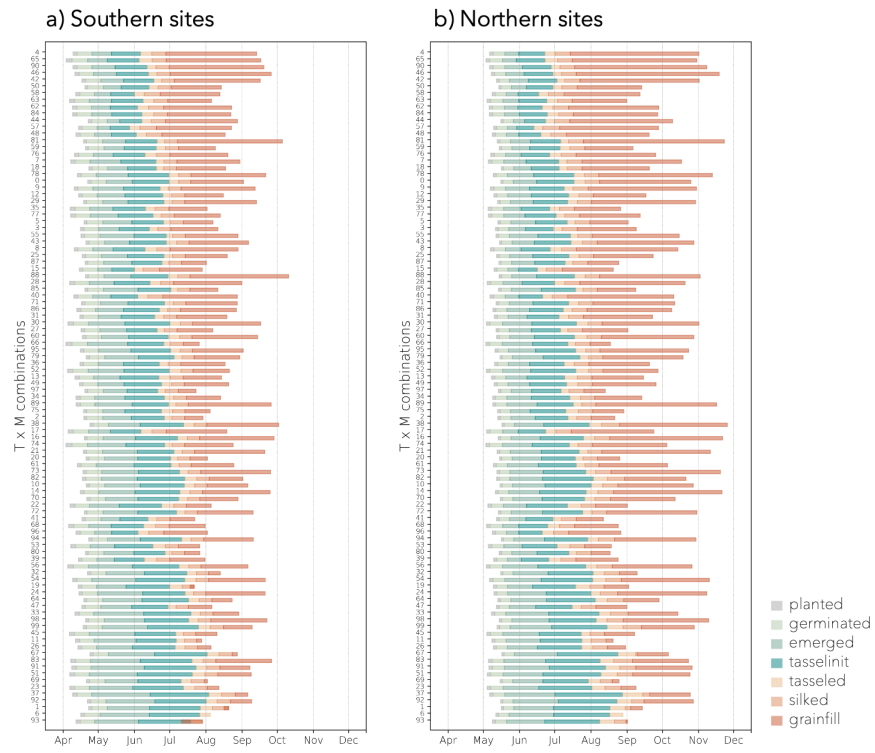


Figure S5: Start time and duration of each phenological stage across  $T \times M$  combinations, averaged across all simulation sites for a) southern sites versus b) northern sites, ranked by overall performance, with the highest performers listed towards the top.

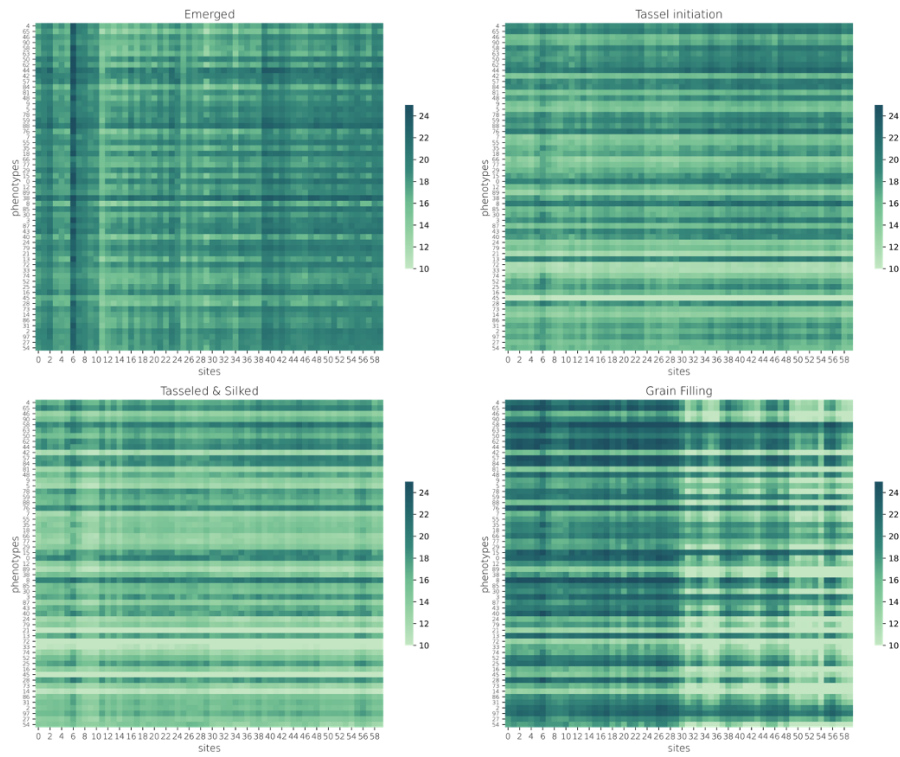


Figure S6: Net photosynthetic rate ( $\mu\text{mol CO}_2 \text{ m}^{-2} \text{ sec}^{-1}$ ) across phenotypes and sites, ranked by the performance of  $T \times M$  combinations, and averaged within each developmental stage.

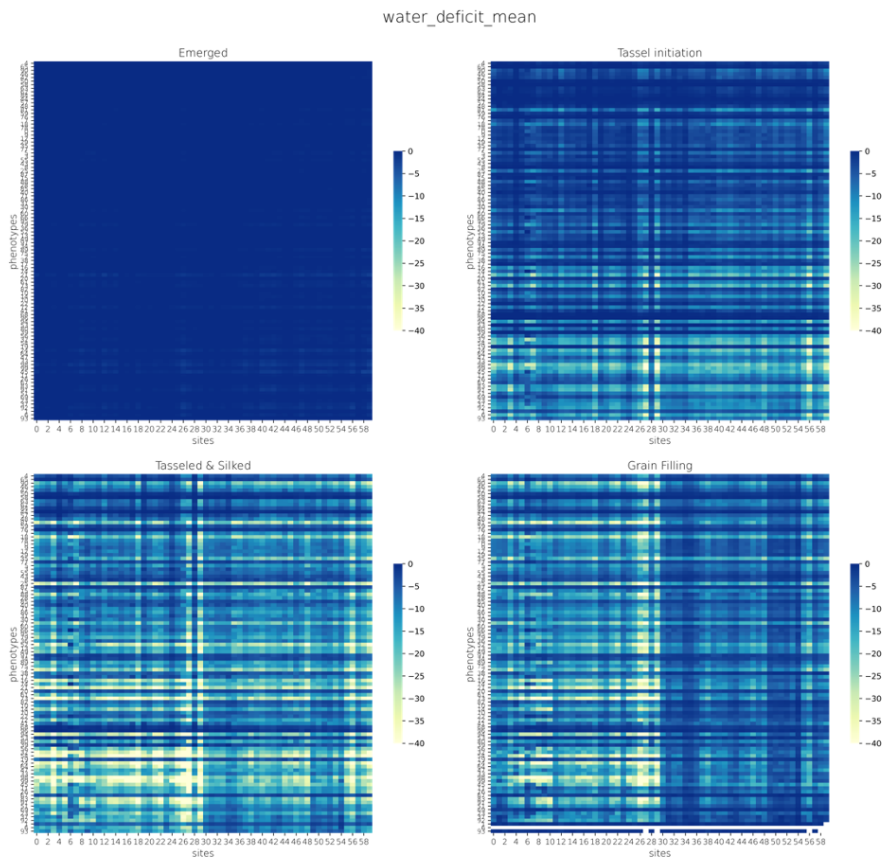


Figure S7: Mean water deficit (g H<sub>2</sub>O) across phenotypes and sites, ranked by the performance of T × M combinations, and averaged within each developmental stage.

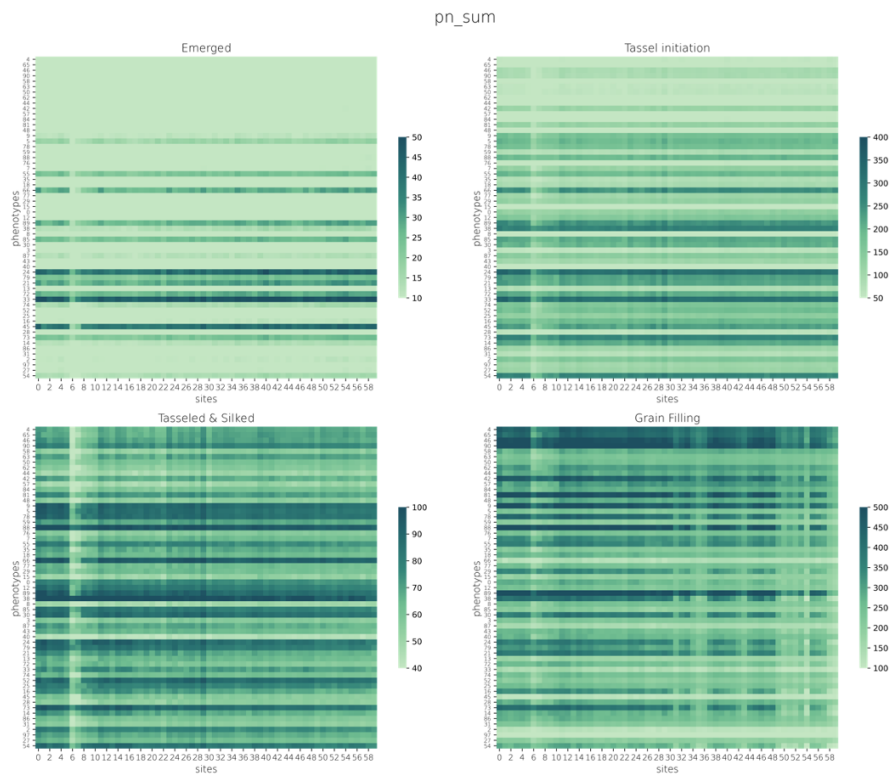


Figure S8: Net carbon gain throughout phenological stage (g C) across phenotypes and sites, ranked by the performance of  $T \times M$  combinations, and averaged within each developmental stage.

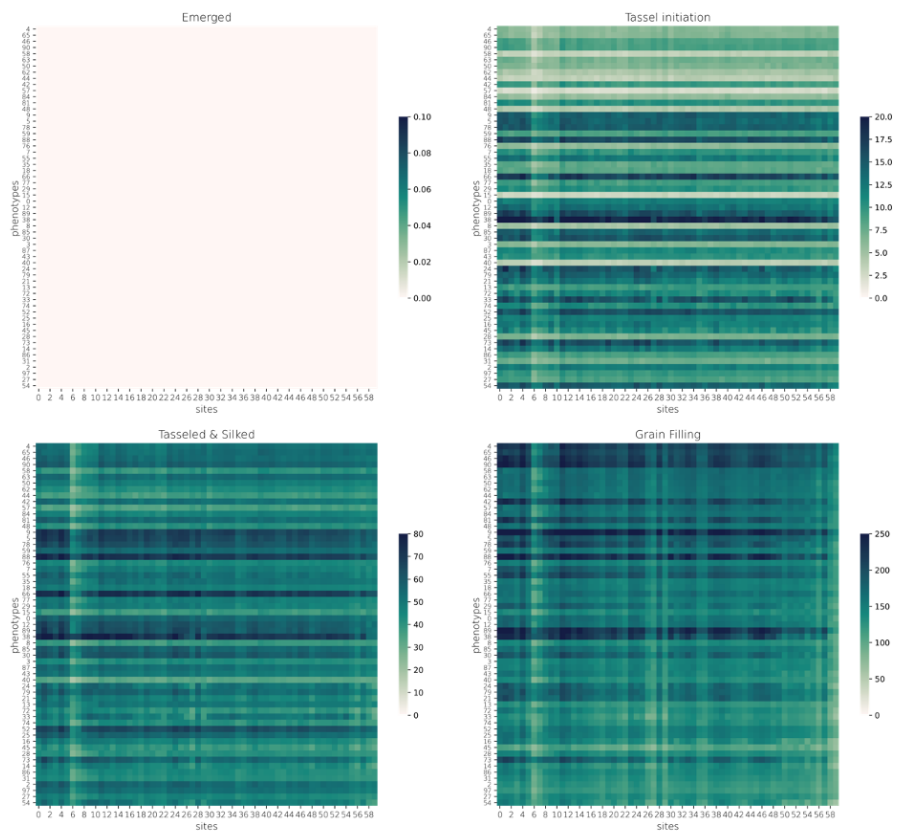


Figure S9: Ear biomass (g/plant) across phenotypes and sites, ranked by the performance of  $T \times M$  combinations, and averaged within each developmental stage.



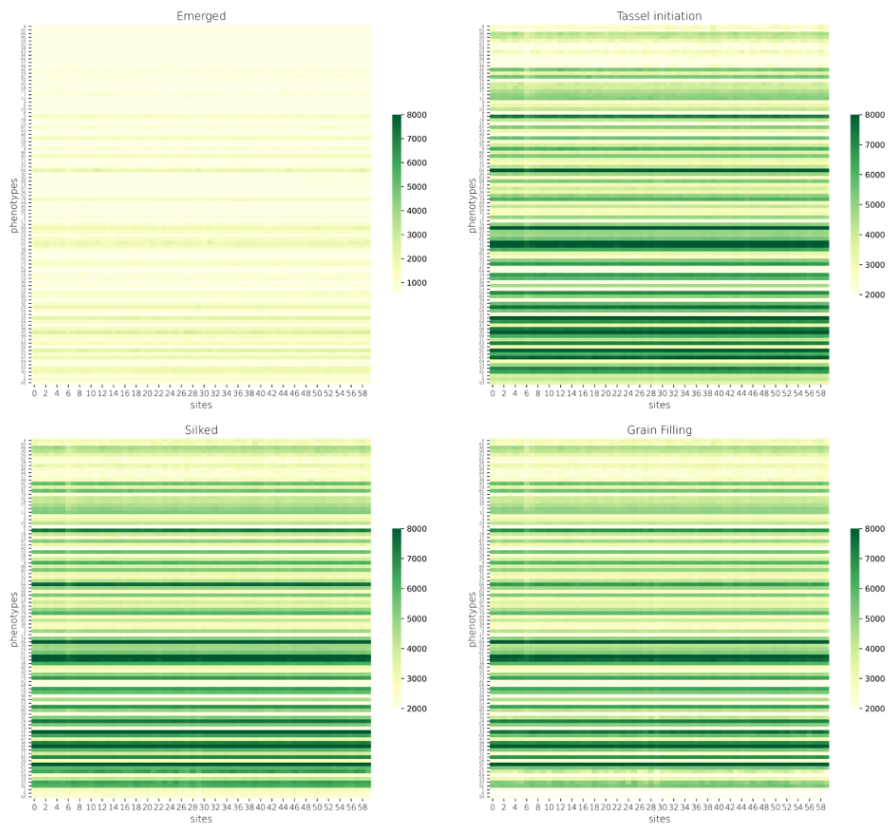


Figure S10: Total leaf area (cm<sup>2</sup>) across phenotypes and sites, ranked by the performance of  $T \times M$  combinations, and averaged within phenological stages..